

The Host Cell ViroCheckpoint: Identification and Pharmacologic Targeting of Novel Mechanistic Determinants of Coronavirus-Mediated Hijacked Cell States

Pasquale Laise^{1,2}, Gideon Bosker¹, Xiaoyun Sun¹, Yao Shen¹, Eugene F. Douglass², Charles Karan², Ronald B. Realubit², Sergey Pampou², Andrea Califano^{2,3,4,5,6,✉}, and Mariano J. Alvarez^{1,2,✉}

¹DarwinHealth Inc, New York, NY, USA.

²Department of Systems Biology, Columbia University Irving Medical Center, New York, NY, USA.

³Herbert Irving Comprehensive Cancer Center, Columbia University Irving Medical Center, New York, NY, USA.

⁴Department of Medicine, Columbia University Irving Medical Center, New York, NY, USA.

⁵Department of Biochemistry & Molecular Biophysics, Columbia University Irving Medical Center, New York, NY, USA.

⁶Department of Biomedical Informatics, Columbia University Irving Medical Center, New York, NY, USA.

Most antiviral agents are designed to target virus-specific proteins and mechanisms rather than the host cell proteins that are critically dysregulated following virus-mediated reprogramming of the host cell transcriptional state. To overcome these limitations, we propose that elucidation and pharmacologic targeting of host cell Master Regulator proteins—whose aberrant activities govern the reprogrammed state of coronavirus-infected cells—presents unique opportunities to develop novel mechanism-based therapeutic approaches to antiviral therapy, either as monotherapy or as a complement to established treatments. Specifically, we propose that a small module of host cell Master Regulator proteins (ViroCheckpoint) is hijacked by the virus to support its efficient replication and release. Conventional methodologies are not well suited to elucidate these potentially targetable proteins. By using the VIPER network-based algorithm, we successfully interrogated 12h, 24h, and 48h signatures from Calu-3 lung adenocarcinoma cells infected with SARS-CoV, to elucidate the time-dependent reprogramming of host cells and associated Master Regulator proteins. We used the NYS CLIA-certified Darwin OncoTreat algorithm, with an existing database of RNASeq profiles following cell perturbation with 133 FDA-approved and 195 late-stage experimental compounds, to identify drugs capable of virtually abrogating the virus-induced Master Regulator signature. This approach to drug prioritization and repurposing can be trivially extended to other viral pathogens, including SARS-CoV-2, as soon as the relevant infection signature becomes available.

Coronavirus | Regulatory networks | Master regulator | Anti-viral drugs

Correspondence: acc2248@cumc.columbia.edu
malvarez@darwinhealth.com

Introduction

SARS-CoV is an enveloped, positive-sense, single-stranded RNA virus of the genera *Betacoronavirus* introduced into the human population from an animal reservoir and culminating in a lethal epidemic in 2002-03, affecting 8,098 indi-

viduals, 774 of whom died (9.6%)(1). The virus shares 79% genome sequence identity with SARS-CoV-2, which is responsible for the current COVID-19 pandemic(2). SARS-CoV can generate a rapid inflammatory cascade eventually leading to pneumonia or severe acute respiratory syndrome (SARS), characterized by diffuse alveolar damage, extensive disruption of epithelial cells and accumulation of reactive macrophages(3). Similar to SARS-CoV-2, SARS-CoV spike protein S binds to angiotensin converting enzyme 2 (ACE2), which is widely expressed on the cell membrane of oral, lung, and nasal mucosa epithelial cells, arterial smooth muscle and venous endothelial cells, as well of other organs, including stomach, small intestine, colon, skin, lymph nodes, spleen, liver, kidney, and brain(4). Supportive care—including prevention of Acute Respiratory Distress Syndrome (ARDS), multi-organ failure, and secondary infections—remains the foundational approach for managing serious infections caused by coronaviruses, although preliminary analysis of a recently-reported, prospective, randomized, placebo-controlled trial, suggests that patients receiving remdesivir recovered faster than those receiving placebo(5–7). Despite early optimism and approval on May 1st, 2020 of remdesivir for emergency use in hospitalized patients with COVID-19, no other specific antiviral treatment has been proven to be effective in randomized, placebo-controlled trials(5, 6). Consequently, there remains a formidable unmet need to identify pharmacologic treatments, alone or in combination—directly targeting either viral mechanisms and/or host cell factors—that significantly inhibit viral replication and, by extension, minimize progression of target organ failure associated with COVID-19.

Current efforts focusing on antiviral drug discovery can be summarized as belonging to two broad strategies: (a) disrupting the synthesis and assembly of viral proteins or (b) targeting host proteins and mechanisms required by the viral replication cycle. The first strategy has yielded drugs targeting (i) viral proteases, required for processing of the virus large

replicase polyprotein 1a, producing non-structural proteins involved in viral transcription and replication(5, 8); (ii) RNA-dependent RNA-polymerase, using guanosine and adenosine analogs, as well as acyclovir derivatives; (iii) virus helicases; (iv) viral spike proteins, with antibodies, peptide decoys and carbohydrate-binding agents; and (v) structural proteins such as those maintaining ion channel activity of CoV E protein and RNA-binding affinity of CoV N protein(5, 6, 9, 10). Although virus-targeting approaches have the advantage of being specific, and, therefore, generally offer acceptable toxicity profiles, targeting viral products typically restricts the applicability of antiviral agents to only one, or only a few, closely related virus species. Moreover, due to the high mutation rate of viral genomes, such drugs are prone to rapid virus adaptation by resistant strain selection(11, 12). Considering the time required to develop new pharmacologic agents, this strategy has proven unsuitable to address new viral epidemics and pandemics in real time.

In contrast, targeting host cell proteins, especially at an early stage when viral hijacking of host mechanisms may still be reversible, may have more universal and longer term value because the same host factors may be required by multiple, potentially unrelated viral species and because host target proteins mutate far less rapidly than viral proteins, thereby limiting emergence of drug resistance(13). Unfortunately, pharmacologic targeting of host factors is more commonly associated with toxicity, thereby limiting clinical application of many drugs identified as potential anti-viral agents *in vitro*, for instance, with anti-CoV drugs EC_{50} markedly exceeding their maximum tolerated serum concentration (C_{max})(5). Despite these translational challenges, current approaches to target host proteins are primarily based on either boosting innate anti-viral immune response, in particular interferon response, or targeting proteins and processes mediating viral infection, such as ACE2 receptors(14), cell surface and endosomal proteases(15), and clathrin mediated endocytosis(16). Moreover, broad availability of high-throughput screening approaches has allowed the purposing and repurposing of drugs based on their effect on virus replication(16–19), leading to identification of several anti-coronavirus candidates, such as chloroquine, tamoxifen, dasatinib and lopinavir, among others(16, 19). Yet, this approach is limited by the idiosyncratic nature of the *in vitro* models used in antiviral screens and by drug concentrations that may not be achievable in patients(5).

More recently, systems biology approaches, including temporal kinome analysis(20) and proteomics(21–24), have also been used to identify protein kinases—and associated pathways—modulated in response to virus infection, as well as to generate virus-host protein-protein interactomes (PPI). These methods also present an opportunity to develop and test host-targeting therapeutic approaches that apply functional genomics to the “infected system as a whole.”(24) The output of these predictions can be used to direct drug repurposing efforts(21–23) and to design more focused *in vitro* screens, with models that better recapitulate disease patho-

physiology, such as primary cells, organoids or 3D organ-on-chip systems(25).

Coronaviruses have been shown to extensively hijack the cellular machinery of host cells they infect; as one example, this class of viruses induces arrest in S phase, allowing them to benefit from physiological alterations they induce in host cells that enhance their reproductive rate(26). As shown for other physiologic(27–29) and pathologic cell states—among them, cancer(30–34), neurodegeneration(35, 36), and diabetes(29)—we propose that such transcriptionally “locked” states are established by the virus and maintained by a handful of Master Regulator (MR) proteins, organized within a highly auto-regulated protein module, or checkpoint (see Califano & Alvarez(30) for a recent perspective). For simplicity, in a viral infection context, we will call such modules “ViroCheckpoints.” Accordingly, we propose that aberrant, virus-mediated activation of a ViroCheckpoint is ultimately responsible for creating a transcriptionally “locked” cellular context that is primed for viral replication and release. We thus propose ViroCheckpoint activity reversal as a potentially valuable therapeutic strategy for pharmacologic intervention.

Here we show that time-dependent, SARS-CoV-mediated ViroCheckpoints—and the specific MR proteins of which they are comprised—can be effectively elucidated by network-based analysis using the Virtual Inference of Protein activity by Enriched Regulon (VIPER) algorithm(37). More importantly, once the MR protein identity is available, drugs can be effectively and reproducibly prioritized based on their ability to invert the activity of ViroCheckpoint MR proteins, using the OncoTreat algorithm(34), a NYS CLIA-certified algorithm that is used routinely on cancer patients at Columbia University.(38)

Accurate identification of virus-dependent MR proteins permits deployment of the same OncoTreat-based methodological approach for mechanism-based repurposing or development of new drugs with potential anti-viral activity. To avoid confusion, we will use the term “ViroTreat” to indicate the virus-specific version of OncoTreat. Specifically, ViroTreat uses the full repertoire of virus-induced MR proteins in the ViroCheckpoint as a reporter assay to identify drugs capable of reversing its activity(34), thereby preventing emergence of or abrogating the virus-mediated transcriptional locked state. While limited by the availability of data on SARS-CoV-2, including of infection in an appropriate pathophysiologic cell context, we provide proof of concept that this approach can be applied to prioritizing FDA-approved and late-stage investigational drugs representing potential antiviral agents for SARS-CoV based on infection in cancer-related lung epithelial cells.

Results

Elucidating MRs of SARS-CoV infection in lung epithelial cells. To identify candidate MR proteins that mechanisti-

cally regulate the host cell gene expression signature induced by SARS-CoV infection (i.e. the SARS-CoV ViroCheckpoint), we applied the VIPER algorithm to a previously-published, microarray-based gene expression signature of a Calu-3 lung adenocarcinoma cell clone expressing elevated ACE2 levels, compared to the parental line, at 12h, 24h, and 48h following infection with SARS-CoV at MOI = 0.1(39). A total of 6,054 regulatory proteins were considered in the analysis, including 1,793 transcription factors (TFs), 656 co-transcription factors (co-TFs), and 3,755 signaling proteins (SP).

Similar to a highly-multiplexed gene reporter assay, VIPER measures the activity of an individual protein based on the enrichment of its positively regulated and repressed targets in genes that are over- and under-expressed in a specific cell state, compared to a control(37). We have shown that VIPER can accurately measure the activity of >70% of regulatory proteins and, as a result, the algorithm has been used to elucidate MRs of both pathologic(31–33, 35, 36, 40, 41) and physiologic cell states(27–29) that have been experimentally validated. Moreover, VIPER-inferred protein activity has been shown to provide a better biomarker of cell phenotype than the original transcriptional profile(30, 34, 42, 43); and, importantly, is a better reporter for validating clinically relevant drug sensitivity(44). Accordingly, VIPER requires a differential expression signature for each sample to be analyzed and a regulatory model comprising the transcriptional targets of each regulatory protein. For the former, we computed a differential gene expression signature for each SARS-CoV infected sample, by comparing it to three 12h mock control replicates. For the latter, we leveraged a transcriptional regulatory model (interactome) generated by ARACNe(45) analysis of 517 samples in the lung adenocarcinoma cohort of The Cancer Genome Atlas (TCGA)(37). Use of a cancer-related interactome is well justified as we have shown that protein transcriptional targets are highly conserved between cancer and normal cells(28).

The analysis revealed $n = 236$ proteins, whose activity was significantly affected by SARS-CoV infection in at least one time point ($p < 10^{-5}$, Bonferroni Corrected (BC), see Supplementary Table 1). Examination of the top 10 activated MR proteins at each of the evaluated time-points (Fig. 1a) revealed the presence of canonical cell-cycle regulators, including (a) cyclins (CCNA2), and other proteins involved in G1/S transition(46) (E2F8 and UHRF1); (b) S-phase proteins, such as topoisomerases (TOP2A(47)) and other factors involved in S-phase cell cycle arrest(48) (CHEK1, GTSE1); (c) mitotic checkpoint proteins(49) (BUB1B, KIF11 and NDC80); and (d) proteins involved in nucleotide synthesis (GMPS). These showed significant activation as early as 12h after SARS-CoV infection. In contrast, established innate immune response proteins were also found among the top activated MRs, including IFN-induced factors(50) (MX1, IRF9 and IFI27) but their activation became most evident only at the latest time point (48h). Interestingly, some proteins previously identified as key tumor MRs were strongly activated,

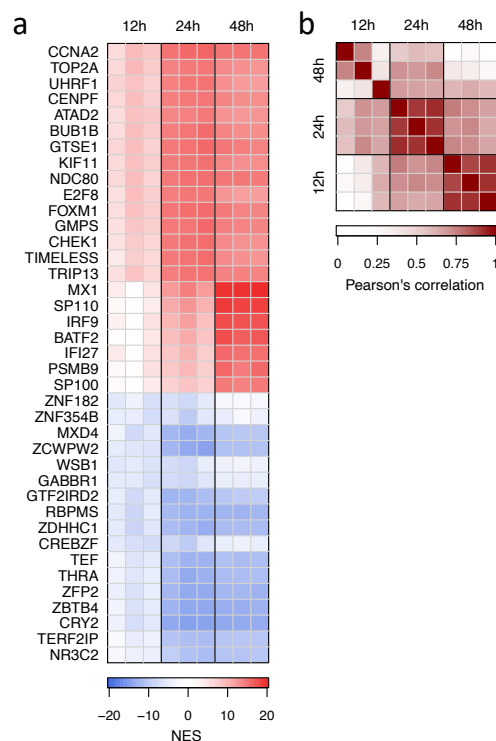


Fig. 1. SARS-CoV-induced ViroCheckpoint in Calu-3 lung adenocarcinoma cells. (a) Heatmap showing the VIPER-inferred protein activity, expressed as normalized enrichment score (NES), for the top 10 most activated and the top 10 most inactivated proteins in response to SARS-CoV infection for each of the three time points. (b) Heatmap showing the similarity between the SARS-CoV induced protein activity signatures, expressed as Pearson's correlation coefficient.

such as FOXM1 and CENPF(33, 51), although this may be a byproduct of the cancer related nature of the Calu-3 cells used in the infection assays.

We then systematically evaluated whether viral infection could affect host proteins known to be involved in SARS-CoV host-pathogen protein-protein interactions (PPI). We based this analysis on a set of 36 proteins previously identified by high-throughput yeast-2-hybrid screen and validated by luciferase assays(23). Of the 36, 12 were represented among our set of 6,054 regulons and could thus be assessed for enrichment in SARS-CoV-induced differentially active proteins. Despite the low statistical power of a test based on only 12 proteins, enrichment was statistically significant for the 12h activity signature ($p < 0.01$, Supplementary Fig. 1a). Enrichment was borderline non-significant at 24h ($p = 0.08$), and not significant at 48h (Supplementary Figs. 1b and c).

To increase the test's sensitivity, we leveraged a larger set of proteins identified as PPI for 26 of the 29 proteins coded by the closely related SARS-CoV-2 virus, as identified by mass-spec analysis of pull-down assays(21). Of 332 host proteins identified by that analysis, 89 were represented among those analyzed by VIPER. Confirming the prior results, enrichment was highly significant ($p_{12h} < 10^{-5}$ by 2-tail aREA test(37); $p_{24h} < 0.01$ and $p_{48h} < 0.001$ by 1-tail aREA test, see Supplementary Fig. 1g, k and l, respectively). Interestingly, while enrichment was significant at all three time

points, ($p < 0.01$, 1-tail aREA test, Supplementary Fig. 1j–l), several of the human SARS-CoV-2 PPIs activated at 12h became inactivated at later time points (Supplementary Fig. 1h–i).

Correlation analysis showed a gradual shift in protein-activity signatures from 12h to 48h after infection (Fig. 1b), suggesting dynamic activation and inactivation of a diverse repertoire of genetic programs by virus-host interaction and thus dynamic transition across multiple, time-dependent ViroCheckpoints. To gain insight into the biological programs most profoundly affected by SARS-CoV infection, we performed Gene-Set Enrichment Analysis (GSEA)(52) of a set of 50 biologically-relevant hallmark gene-sets from MSigDB(53) in differentially active, infection-mediated proteins (Fig. 2). The analysis identified four time-dependent program classes including: (a) cell cycle programs, consistently up-regulated at all three time points; (b) immune-related programs, associated with interferon response, inflammatory response, TNF- α , and IL-6/JACK/STAT3 signaling, which were progressively upregulated over time; (c) DNA repair pathways and (d) PI3K/AKT/mTOR programs more strongly activated at 12h (Fig. 2).

Consistent with the multifarious effects that coronaviruses are known to exert through their complex, synchronized modulations of cell cycle progression, interferon antagonism, interleukin 6 and 8 induction, and host protein synthesis(26), these findings disclose a time-dependency, with early vs. late activation of protein signatures each linked to a distinct set of biofunctional hallmarks resulting from a virus-governed reconfiguration of the host cell's regulatory state, with alterations in cell cycle during the initial post-infection phase, followed by a phase characterized by ignition of pro-inflammatory cytokine signaling pathways.

ViroTreat analysis of SARS-CoV infected cells identifies novel therapeutic targets for drug repurposing.

We have previously developed and validated a systematic approach (OncoTreat) for identifying drugs and compounds capable of reversing the aberrant activity of all Tumor Checkpoint MRs, representing mechanistic determinants of cell state, on a patient by patient basis(34). As a direct result of the high reproducibility demonstrated by VIPER,(37) the test has been certified by the NYS-CLIA laboratory and is available in the United States from the Columbia University Laboratory of Personalized Genomic Medicine(38); and, in China, from the Xiamen Encheng Group Ltd.

OncoTreat is used routinely to assess potential therapy for cancer patients who are progressing on standard of care, as part of the Columbia Precision Oncology Initiative(54). Despite the fact that it was originally developed for deployment and drug prioritization in the setting of precision oncology, the OncoTreat methodology is fully generalizable and can be applied to any state transition and any drug collection, including transitions related to and induced by viral infection. To avoid confusion, we will use the term ViroTreat to refer to the algorithm when used to identify antiviral drugs (see

description in Fig. 3).

ViroTreat requires a tissue-matched drug perturbation database. For this analysis, we had previously generated a collection of RNASeq profiles of NCI-H1793 lung adenocarcinoma cells, at 24h following treatment with a repertoire of 133 FDA approved and 195 late-stage (Phase 2 and 3) drugs—primarily used in or developed for the oncology setting—at their highest subtoxic concentration (48h IC_{20}) or maximum serum concentration (C_{max}), whichever is lower. RNASeq data was generated using a fully automated, 96-well based microfluidic technology called PLATE-Seq(55) (Supplementary Table 2). Selection of the NCI-H1793 cell line as an adequate model for the analysis was based on the significant overlap of SARS-CoV infection MR proteins with proteins differentially activated in this cell line ($p < 10^{-28}$, 10^{-38} , and 10^{-24} at 12h, 24h and 48h after infection, by 1-tail aREA test; see Supplementary Fig. 2). In addition, the main rationale for these assays is the elucidation of protein-level MoA of a drug repertoire and MoA is generally well-recapitulated in lineage matched cells(56).

Using this predictive model, ViroTreat prioritized 44 FDA-approved drugs and 49 investigational compounds in oncology, based on their ability to significantly invert the ViroCheckpoint protein activity signature, at one or more of the 3 evaluated time-points following infection ($p < 10^{-10}$, BC; see Supplementary Table 3). Based on this analysis, two FDA-approved drugs—the CDK inhibitor palbociclib and the MEK inhibitor trametinib—and 4 investigational compounds, including three MAP kinase and one AKT/CHEK1 inhibitors, were able to significantly invert the ViroCheckpoint activity at all three time-points ($p < 10^{-10}$, BC, Fig. 4a). In addition, six FDA-approved drugs and seven investigational compounds demonstrated the capacity to invert the ViroCheckpoint protein activity pattern at the two earliest time points (12h and 24h, $p < 10^{-10}$, BC, Fig. 4a); while two FDA-approved drugs—the ALK and EGFR inhibitors brigatinib and osimertinib—and five investigational compounds were predicted to significantly invert the MR signature identified at later time points (24h and 48h, $p < 10^{-10}$, BC, Fig. 4a).

Consistent with the pathways enrichment analysis (Fig. 2), several drug families were enriched among the top ViroTreat predictions, including MAP kinases, PI3K/AKT/mTOR, CDK and other cell cycle-related drugs; HDAC and bromodomain protein inhibitors; proteasome and HSP90 inhibitors; and NF- κ B and JAK inhibitors (Fig. 4a).

Of special clinical relevance in the context of the COVID-19 pandemic, ViroTreat independently identified the Selective Inhibitor of Nuclear Export (SINE) drug selinexor—FDA-approved for the treatment of relapsed or refractory multiple myeloma—as an extremely potent inverter of SARS-CoV induced ViroCheckpoint activity, in particular, at 12h and 24h time points after infection ($p_{12h} < 10^{-16}$ and $p_{24h} < 10^{-19}$, BC, Fig. 4).

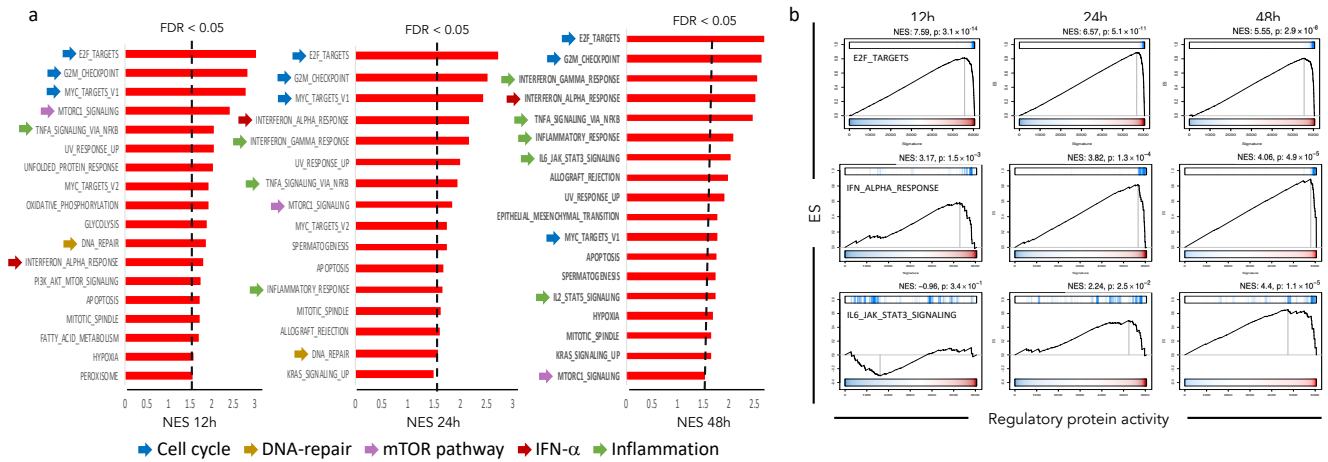


Fig. 2. Biological programs activated by SARS-CoV infection. (a) Hallmark gene-sets from MSigDB significantly enriched ($FDR < 0.05$) in proteins activated at 12h, 24h and 48h after SARS-CoV infection. The bars indicate the GSEA-estimated Normalized Enrichment Score (NES). Pathways and processes related to cell cycle progression and cell proliferation, DNA-repair, mTOR, IFN- α and inflammation are indicated by blue, yellow, purple, red and green arrows, respectively. (b) GSEA plots showing the enrichment of E2F-targets, IFN- α -response and IL6/JAK/STAT pathway hallmark gene-sets on the differential activity of 6,054 regulatory proteins at 12h, 24h and 48h after SARS-CoV infection. The x-axis shows the regulatory proteins sorted from the most inactivated (left), to the most activated (right) in response to viral infection. The y-axis shows the enrichment score estimated by GSEA. The blue vertical lines indicate the proteins annotated as part of each of the analyzed biological programs/pathways.

Discussion

ViroTreat presents an application of the extensively validated OncoTreat algorithm for targeting MR proteins driving virus-mediated, reprogrammed cell states induced by viral hijacking of the host cell regulatory machinery. It also provides proof-of-concept of the ability to rapidly prioritize drugs capable of abrogating the reprogrammed, transcriptionally-locked state induced by viral infection, responsible for creating an environment permissive to viral replication and release. Our analysis identified 44 FDA-approved and 49 investigational agents capable of virtually abrogating the MR signature—the ViroCheckpoint protein activity pattern—induced by SARS-CoV infection.

Consistent with the observation that coronaviruses interfere with cell cycle progression to benefit from the physiology of host cells arrested in S phase(26), we show SARS-CoV infection-induced activation of MRs involved in cell cycle progression and DNA repair pathways. Notably, it has been reported previously that coronaviruses inhibit the pRb tumor suppressor protein, inducing infected cell to progress rapidly from G_1 and to arrest the host cell in S phase(57). SARS-CoV further favors host cell arrest in S phase by inhibiting CDK4 and CDK6 kinase activity(58). We also observed activation of PI3K/AKT/mTOR pathway proteins, suggesting that SARS-CoV—similar to other viruses(59), including +ssRNA viruses like chikungunya(60), hepatitis C(61), west nile(62) and dengue(63), as well as other RNA respiratory viruses like influenza(64) and the respiratory syncytial virus(65)—might subvert mTOR pathway activity. Indeed, temporal kinome analysis of human hepatocytes infected with MERS-CoV had previously revealed changes in MAPK and PI3K/AKT/mTOR pathways(20). Finally, we observed activation of proteins involved in innate immunity, including interferon response and pro-inflammatory pathways, which have been also previously described for coronaviruses(26).

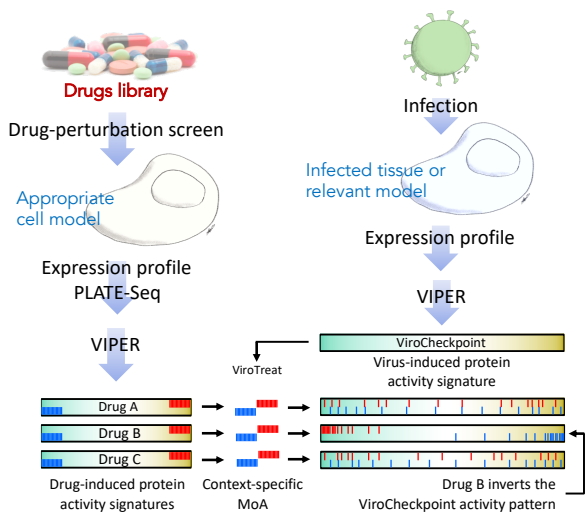


Fig. 3. ViroTreat diagram. ViroTreat requires two components: (A) a context-specific drug Mechanism of Action (MoA) database, which is generated by perturbing an appropriate cell model with therapeutically relevant drug concentrations, followed by VIPER analysis of the drug-induced gene expression signatures and identification of the top most differentially active proteins, both activated and inactivated in response to the drug; and (B) the specific virus-induced protein activity signature—where the most differentially active proteins constitute the ViroCheckpoint—dissected by VIPER analysis of a gene expression signature, obtained by comparing an infected tissue or relevant model with non-infected mock controls. ViroTreat then predicts the effect of the drugs on the ViroCheckpoint by matching their MoA with the virus-induced protein activity signature, and quantifies the inverse enrichment using the aREA algorithm. The diagram shows 3 drugs, where only drug B, by activating the host proteins that are being inactivated during virus infection, and inactivating the proteins that are being activated by the virus infection, effectively acts by inverting the ViroCheckpoint activity pattern; and, therefore, would be prioritized as a host cell-targeted antiviral therapeutic option.

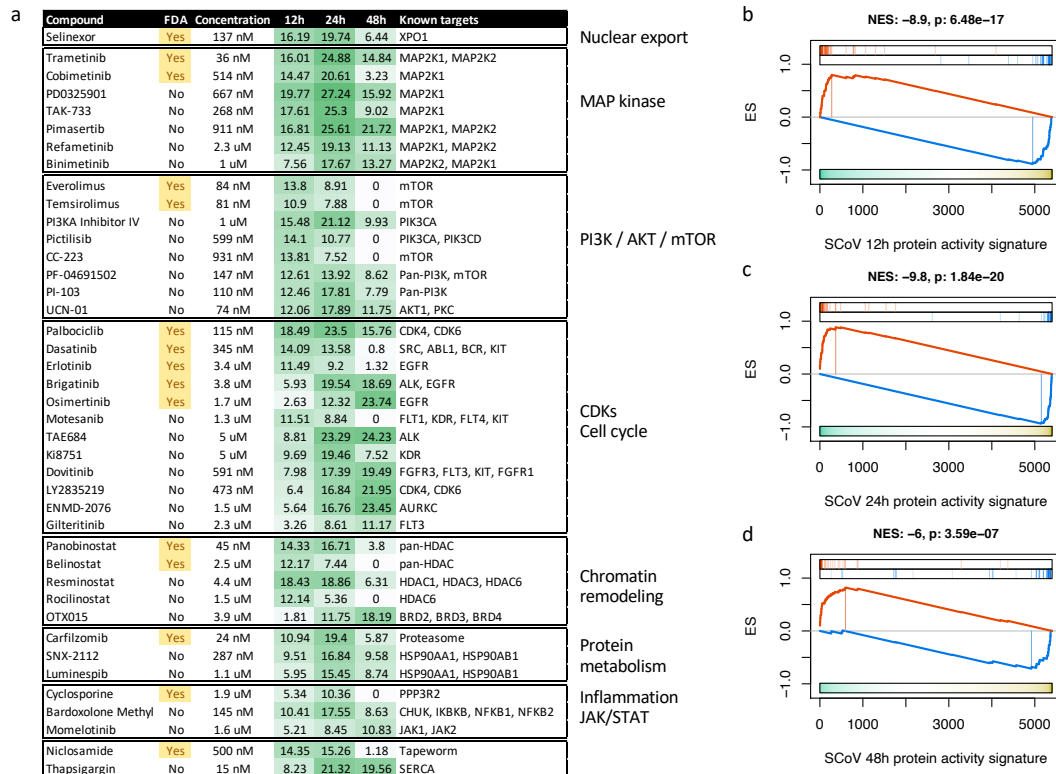


Fig. 4. Top drugs and compounds identified by ViroTreat. (a) Table of FDA-approved drugs and investigational compounds identified by ViroTreat as significantly inverting the pattern of activity of the SARS-CoV induced checkpoint ($p < 10^{-10}$, BC) for at least one of the three analyzed time points, and being simultaneously significant ($p < 10^{-5}$, BC) for at least another time point. The drugs and compounds were organized in blocks according to the biological role or pathway membership of their primary target protein. For each block, the drugs and compounds significant for each time point ($p < 10^{-10}$, BC), were sorted by their ViroTreat significant level for 12h, followed by 24h and 48h. FDA-approved drugs were reported prior to investigational compounds. The table also shows the concentration used to perturb NCI-H1793 cells, the ViroTreat significance level, as $-\log_{10}(p\text{-value})$, BC, indicated by the green heatmap, and the primary target for each of the significant drugs and compounds. (b–d) GSEA plots showing the enrichment of the top 25 proteins most activated (red vertical lines), and the top 25 proteins most inactivated (blue vertical lines), in NCI-H1793 cells in response to selinexor perturbation, on the protein activity signatures induced by SARS-CoV infection of Calu-3 cells (x-axis) for 12h (b), 24h (c) and 48h (d). NES and p -value, estimated by 2-tail AREA test, are indicated on top of each plot.

While formal experimental validation is still required, there are several positive indications this approach may be effective. Specifically, drugs for SARS-CoV most highly prioritized by ViroTreat were highly consistent, at least based on their primary target proteins, with biological programs and pathways known to be modulated by coronavirus infection(26, 66). Notably, in this regard, cell cycle progression/proliferation, PI3K/AKT/mTOR, innate immunity and inflammation are well represented among the primary target proteins for those pharmacologic agents strongly predicted by ViroTreat to possess host cell-targeted, antiviral effects.

A literature search revealed that many of the oncology drugs and compounds identified by ViroTreat have been considered previously for their potential antiviral effects. For instance, the MAPK inhibitor trametinib, one of the top ViroTreat hits for SARS-CoV, was shown to inhibit MERS-CoV replication *in vitro*(5, 20), as well as influenza A virus both *in vitro* and *in vivo*(67). Similarly, everolimus, an mTOR inhibitor identified by ViroTreat, has also been shown to inhibit MERS-CoV(5, 20) and cytomegalovirus(68) replication *in vitro*, as well as to reduce incidence of cytomegalovirus infections following kidney transplant(69). Among tyrosine kinase inhibitors identified by ViroTreat, dasatinib was previously described to inhibit MERS-CoV(5, 19) and HIV-1(70)

replication *in vitro*; while erlotinib was shown to inhibit dengue(71), hepatitis C(72) and ebola(73) replication. The HSP90 inhibitors SNX-2112 and luminespib, as well as the sarco/endoplasmic reticulum Ca^{2+} ATPase inhibitor thapsigargin, all identified by ViroTreat as inverters of the SARS-CoV induced checkpoint, have been shown to inhibit herpes simplex(74), chikungunya(75), foot and mouth disease virus(76), respiratory syncytial virus(77), rhinovirus(78) and hepatitis A virus replication(79).

Finally, ViroTreat independently identified the SINE drug molecule selinexor—an FDA-approved agent for the treatment of relapsed or refractory multiple myeloma—as an extremely potent inverter of SARS-CoV-induced ViroCheckpoint activity. Selinexor is a potent and highly-specific inhibitor of XPO1 activity, which leads to nuclear retention of its cargo proteins containing leucine rich Nuclear Export Signals. Based on experimental studies performed by Karyopharm Therapeutics Inc., low Selinexor concentrations (100 nM) inhibited viral replication by 90% in green monkey kidney Vero cells infected with SARS-CoV-2(80). As a result of these observations and data, which are consistent with the ViroTreat prioritization of selinexor we report in this study, a randomized, placebo-controlled Phase 2 clinical study (NCT04355676 and NCT04349098), evaluat-

ing low dose oral selinexor in hospitalized patients with severe COVID-19 has been initiated and is currently enrolling patients, with results anticipated to be reported by August 31st, 2020(80).

This analysis has several limitations that partially restrict its value as proof of concept. Specifically, infection was conducted in a cancer cell line, rather than in a more physiologically relevant context, such as in primary bronchial or alveolar epithelial cells. In addition, drug perturbations were also performed in a cancer cell line context, thus potentially introducing undesired confounding factors, even though use of mock controls for the infection, and vehicle control for the drug perturbations, from the same cancer cell line should have eliminated most of the cancer-related bias and cell line idiosyncrasies. As a result, extrapolation of this approach to the clinic may be limited by the following assumptions: (a) that the host cell regulatory checkpoint hijacked by the virus is conserved between the Calu-3 adenocarcinoma cell line and the normal alveolar or bronchial epithelial cells *in vivo*; and (2) that the drugs' and compounds' MoA is conserved between the NCI-H1793 lung adenocarcinoma cells and normal lung epithelial cells *in vivo*. Moreover, while for the generation of the perturbational data and the context-specific MoA database we used subtoxic drug concentrations that, in most cases, were well below the maximum tolerated dose for all drugs and compounds, the relevant pharmacologic concentration for their deployment as antiviral therapy may be much lower than the original recommended concentration for their use as anti-cancer drugs.

Further research is necessary to benchmark the ViroTreat approach. Specifically, better reporters of SARS-CoV infection should be established, ideally directly from nasopharyngeal swabs or bronchial lavage of SARS-CoV patients. More relevant to the current pandemic, such samples are starting to emerge from COVID-19 patients and may lead to elucidation of critical entry points for COVID-19 therapeutic intervention. Similarly, drug profiles should be generated in a more physiologic context, including primary airway epithelial cells. It is also important to establish whether virus-induced transcriptional lock states are similar across all cell and tissue contexts infected by the virus, or whether the hijacked states are cell context-specific. Finally, appropriate environments for *in vitro* and *in vivo* validation of prioritized drugs should be developed(56).

To our knowledge, this is the first time a virus-induced MR module (i.e., the ViroCheckpoint) is proposed as a pharmacological target to abrogate the virus's ability to hijack the cellular machinery of host cells, a strategy that coronaviruses are known to employ to prime the host cell environment so it is amenable to viral replication and release(26). In addition, ViroTreat represents a unique method for the systematic and quantitative prioritization of mechanism-based, host-directed drugs capable of abrogating this critical, and previously unaddressed component of viral infection. If effectively validated, this approach presents several advantages: First, ViroTreat is tailored to target the entire repertoire of host pro-

teins hijacked by the virus to create a permissive environment, rather than a single host or viral protein. As such, we anticipate drugs identified by ViroTreat to have more universal applications, including being effective against a broader viral repertoire, while also being more effective at eluding virus adaptation mechanisms arising from rapid mutation under drug selection stress. Indeed, drug-mediated reprogramming of host cell to a transcriptional state that confers resistance against coronavirus-induced reprogramming presents the opportunity to identify drugs that are potentially effective for a broader class of viruses, as long as they share similar pathobiological strategies for host cell takeover. Second, the ViroTreat analysis can be performed expeditiously—as soon as the ViroCheckpoint signature of a novel virus becomes available. Therefore, this methodology is especially well-suited to the urgency characteristic of epidemics and pandemics.

Developing effective treatments for respiratory tract infections—i.e., those that reduce such hard end points as hospitalization, need for mechanical ventilation, and mortality—exclusively through direct viral targeting has been historically challenging. Drugs identified specifically for host cell-targeting have the potential therapeutic advantage of acting in a mechanistically complementary—even synergistic—way with readily available antivirals, thereby suggesting roadmaps for developing and testing combination regimens that may mitigate viral replication by acting upon the infected system as a whole. Such multi-mechanistic pharmacologic approaches targeting both the virus and host cell proteins that are critically dysregulated as a result of viral infection may be required to optimize clinical outcomes, especially in challenging and vulnerable patients exposed to lethal pathogens with high virulence and viral load.

ACKNOWLEDGEMENTS

We thank Christopher Walker for reviewing selinexor data accuracy and Tatiana Alvarez for original artwork. This research was supported by the following NIH grants to Andrea Califano: R35 CA197745 (Outstanding Investigator Award); U01 CA217858 (Cancer Target Discovery and Development); S10 OD012351 and S10 OD021764 (Shared Instrument Grants).

Author Contributions. Conceptualization and Methodology, P.L., A.C. and M.J.A.; Investigation, P.L., X.S., G.B. and M.J.A.; Formal Analysis, P.L., X.S., Y.S., E.F.D. and M.J.A.; Experimental execution and data generation: C.K., R.R. and S.P.; Original Draft, G.B., A.C. and G.B.; Writing – Review and Editing, P.L., G.B., A.C. and M.J.A.

Competing Financial Interests Statement. P.L. is Director of Single-Cell Systems Biology at DarwinHealth, Inc., a company that has licensed some of the algorithms used in this manuscript from Columbia University. G.B. is founder, CEO and equity holder of DarwinHealth, Inc. X.S. is Senior Computational Biologist at DarwinHealth, Inc. A.C. is founder, equity holder, consultant, and director of DarwinHealth Inc. M.J.A. is CSO and equity holder of DarwinHealth, Inc. Columbia University is also an equity holder in DarwinHealth Inc.

Bibliography

- Joseph S.M. Peiris, Kwok Y. Yuen, Albert D.M.E. Osterhaus, and Klaus Stöhr. The Severe Acute Respiratory Syndrome. *New England Journal of Medicine*, 349(25):2431–2441, dec 2003. ISSN 0028-4793. doi: 10.1056/NEJMra032498.
- Na Zhu, Dingyu Zhang, Wenling Wang, Xingwang Li, Bo Yang, Jingdong Song, Xiang Zhao, Baoying Huang, Weifeng Shi, Roujian Lu, Peihua Niu, Faxian Zhan, Xuejun Ma, Dayan Wang, Wenbo Xu, Guizhen Wu, George F. Gao, Wenjie Tan, and China Novel Coronavirus Investigating and Research Team. A Novel Coronavirus from Patients with Pneumonia in China, 2019. *The New England Journal of Medicine*, 382(8):727–733, 2020. ISSN 1538-4406. doi: 10.1056/NEJMoa2001017.
- John M Nicholls, Leo LM Poon, Kam C Lee, Wai F Ng, Sik T Lai, Chung Y Leung, Chung M Chu, Pak K Hui, Kong L Mak, Wilna Lim, Kin W Yan, Kwok H Chan, Ngai C Tsang, Yi Guan, Kwok Y Yuen, and JS Malik Peiris. Lung pathology of fatal severe acute respiratory syndrome. *The Lancet*, 361(9371):1773–1778, may 2003. ISSN 01406736. doi: 10.1016/S0140-6736(03)13413-7.
- Wenhui Li, Chengsheng Zhang, Jianhua Sui, Jens H Kuhn, Michael J Moore, Shiwen Luo, Swee-Kee Wong, I-Chueh Huang, Keming Xu, Natalya Vasilieva, Akikazu Murakami, Yaqing He, Wayne A Marasco, Yi Guan, Hyeryun Choe, and Michael Farzan. Receptor and viral determinants of SARS-coronavirus adaptation to human ACE2. *The EMBO Journal*, 24(8):1634–1643, apr 2005. ISSN 0261-4189. doi: 10.1038/sj.emboj.7600640.
- Alimuddin Zumla, Jasper F W Chan, Esam I. Azhar, David S C Hui, and Kwok-Yung Yuen. Coronaviruses - drug discovery and therapeutic options. *Nature reviews. Drug discovery*, 15(5):327–47, may 2016. ISSN 1474-1784. doi: 10.1038/nrd.2015.37.
- James M Sanders, Marguerite L Monogue, Tomasz Z Jodkowski, and James B Cutrell. Pharmacologic Treatments for Coronavirus Disease 2019 (COVID-19): A Review. *JAMA*, apr 2020. ISSN 1538-3598. doi: 10.1001/jama.2020.6019.
- NIAID. NIH Clinical Trial Shows Remdesivir Accelerates Recovery from Advanced COVID-19, 2020.
- Yahira M. Báez-Santos, Sarah E. St. John, and Andrew D. Mesecar. The SARS-coronavirus papain-like protease: Structure, function and inhibition by designed antiviral compounds. *Antiviral Research*, 115:21–38, mar 2015. ISSN 01663542. doi: 10.1016/j.antiviral.2014.12.015.
- Guangdi Li and Erik De Clercq. Therapeutic options for the 2019 novel coronavirus (2019-nCoV). *Nature reviews. Drug discovery*, 19(3):149–150, 2020. ISSN 1474-1784. doi: 10.1038/d41573-020-00016-0.
- Adeyemi O. Adedeji and Stefan G. Sarafianos. Antiviral drugs specific for coronaviruses in preclinical development. *Current Opinion in Virology*, 8:45–53, 2014. ISSN 18796265. doi: 10.1016/j.coviro.2014.06.002.
- Nila J. Dharan. Infections With Oseltamivir-Resistant Influenza A(H1N1) Virus in the United States. *JAMA*, 301(10):1034, mar 2009. ISSN 0098-7484. doi: 10.1001/jama.2009.294.
- Nelson Lee and Aeron C. Hurt. Neuraminidase inhibitor resistance in influenza. *Current Opinion in Infectious Diseases*, 31(6):520–526, dec 2018. ISSN 0951-7375. doi: 10.1097/QCO.0000000000000498.
- Simónides I. van de Wakker, Marcel J E Fischer, and Ronald S. Oosting. New drug strategies to tackle viral-host interactions for the treatment of influenza virus infections. *European journal of pharmacology*, 809:178–190, aug 2017. ISSN 1879-0712. doi: 10.1016/j.ejphar.2017.05.038.
- Dong P. Han, Adam Penn-Nicholson, and Michael W. Cho. Identification of critical determinants on ACE2 for SARS-CoV entry and development of a potent entry inhibitor. *Virology*, 350(1):15–25, jun 2006. ISSN 00426822. doi: 10.1016/j.viro.2006.01.029.
- Yanchen Zhou, Punitha Vedantham, Kai Lu, Juliet Agudelo, Ricardo Carrion, Jerritt W. Nunneley, Dale Barnard, Stefan Pöhlmann, James H. McKeown, Adam R. Renslo, and Graham Simmons. Protease inhibitors targeting coronavirus and filovirus entry. *Antiviral Research*, 116:76–84, apr 2015. ISSN 01663542. doi: 10.1016/j.antiviral.2015.01.011.
- Adriaan H de Wilde, Dirk Jochmans, Clara C. Posthuma, Jessika C. Zevenhoven-Dobbe, Stefan van Nieuwkoop, Theo M. Bestebroer, Bernadette G. van den Hoogen, Johan Neyts, and Eric J. Snijder. Screening of an FDA-approved compound library identifies four small-molecule inhibitors of Middle East respiratory syndrome coronavirus replication in cell culture. *Antimicrobial agents and chemotherapy*, 58(8):4875–84, aug 2014. ISSN 1098-6596. doi: 10.1128/AAC.03011-14.
- Miao Xu, Emily M. Lee, Zhexiong Wen, Yichen Cheng, Wei-Kai Huang, Xuyu Qian, Julia Tow, Jennifer Kouznetsova, Sarah C. Ogden, Christy Hammack, Fadi Jacob, Ha Nam Nguyen, Misha Itkin, Catherine Hanna, Paul Shinn, Chase Allen, Samuel G. Michael, Anton Simeonov, Wenwei Huang, Kimberly M. Christian, Alison Goate, Kristen J. Brennan, Ruiji Huang, Menghang Xia, Guo-Li Ming, Wei Zheng, Hongjun Song, and Hengli Tang. Identification of small-molecule inhibitors of Zika virus infection and induced neural cell death via a drug repurposing screen. *Nature medicine*, 22(10):1101–1107, oct 2016. ISSN 1546-170X. doi: 10.1038/nm.4184.
- Lisa M. Johansen, Jennifer M. Brannan, Sue E. Delos, Charles J. Shoemaker, Andrea Stosel, Calli Lear, Benjamin G. Hoffstrom, Lisa Evans Dewald, Kathryn L. Schornberg, Corinne Scully, Joseph Lehár, Lisa E. Hensley, Judith M. White, and Gene G. Olinger. FDA-approved selective estrogen receptor modulators inhibit Ebola virus infection. *Science translational medicine*, 5(190):190ra79, jun 2013. ISSN 1946-6242. doi: 10.1126/scitranslmed.3005471.
- Julie Dyall, Christopher M. Coleman, Brit J. Hart, Thiagarajan Venkataraman, Michael R. Holbrook, Jason Kindrachuk, Reed F. Johnson, Gene G. Olinger, Peter B. Jahrling, Monique Laidlaw, Lisa M. Johansen, Calli M. Lear-Rooney, Pamela J. Glass, Lisa E. Hensley, and Matthew B. Frieman. Repurposing of clinically developed drugs for treatment of Middle East respiratory syndrome coronavirus infection. *Antimicrobial agents and chemotherapy*, 58(8):4885–93, aug 2014. ISSN 1098-6596. doi: 10.1128/AAC.03036-14.
- Jason Kindrachuk, Britini Ork, Brit J. Hart, Steven Mazur, Michael R. Holbrook, Matthew B. Frieman, Dawn Traynor, Reed F. Johnson, Julie Dyall, Jens H. Kuhn, Gene G. Olinger, Lisa E. Hensley, and Peter B. Jahrling. Antiviral potential of ERK/MAPK and PI3K/AKT/mTOR signaling modulation for Middle East respiratory syndrome coronavirus infection as identified by temporal kinome analysis. *Antimicrobial agents and chemotherapy*, 59(2):1088–99, feb 2015. ISSN 1098-6596. doi: 10.1128/AAC.03659-14.
- David E Gordon, Gwendolyn M Jang, Mehdi Bouhaddou, Jiewei Xu, Kirsten Obernier, Kris M. White, Matthew J. O’Meara, Veronica V Rezell, Jeffrey Z Guo, Danielle L Swaney, Tia A. Tummino, Ruth Huettenhain, Robyn M Kaake, Alicia L Richards, Beril Tutuncoglu, Helene Foussard, Jyoti Batra, Kelsey Haas, Maya Modak, Minkyu Kim, Paige Haas, Benjamin J. Polacco, Hannes Braberg, Jacqueline M Fabius, Manon Eckhardt, Margaret Souchery, Melanie J Bennett, Merve Cakir, Michael J. McGregor, Qiongyu Li, Bjørn Meyer, Ferdinand Roesch, Thomas Vallet, Alice Mac Kain, Lisa Miorin, Elena Moreno, Zun Zar Chi Naing, Yuan Zhou, Shiming Peng, Ying Shi, Ziyang Zhang, Wenqi Shi, Ilsa T Kirby, James E Melnyk, John S. Chorbha, Kevin Lou, Shizhong A. Dai, Inigo Barrio-Hernandez, Danish Memon, Claudia Hernandez-Armenta, Jiankun Lyu, Christopher J. P. Mathy, Tina Perica, Kala B. Pilla, Sai J. Ganesan, Daniel J. Saltzberg, Ramachandran Rakesh, Xi Liu, Sara B. Rosenthal, Lorenzo Calviello, Srivats Venkataramanan, Jose Liboy-Lugo, Yizhu Lin, Xi-Ping Huang, YongFeng Liu, Stephanie A. Wankowicz, Markus Bohn, Maliheh Safari, Fatima S. Ugur, Cassandra Koh, Nastaran Sadat Savar, Quang Dinh Tran, Djosh Shengjuler, Sabrina J Fletcher, Michael C. O’Neal, Yiming Cai, Jason C J Chang, David J Broadhurst, Saker Klippsten, Phillip P Sharp, Nicole A. Wenzell, Duygu Kuzuoglu, Hao-Yuan Wang, Raphael Trenker, Janet M. Young, Devin A. Caverio, Joseph Hiatt, Theodore L Roth, Ujjwal Rathore, Advait Subramanian, Julia Noack, Mathieu Hubert, Robert M. Stroud, Alan D. Frankel, Oren S. Rosenberg, Kliment A Verba, David A. Agard, Melanie Ott, Michael Emerman, Natalia Jura, Mark von Zastrow, Eric Verdin, Alan Ashworth, Olivier Schwartz, Christophe D’Enfert, Shaeri Mukherjee, Matt Jacobson, Harmit S Malik, Danica G Fujimori, Trey Ideker, Charles S Craik, Stephen N Floor, James S. Fraser, John D Gross, Andrej Sali, Bryan L Roth, Davide Ruggero, Jack Taunton, Tanja Kortemmo, Pedro Beltrao, Marco Vignuzzi, Adolfo Garcia-Sastre, Kevan M Shokat, Brian K. Shoichet, and Nevan J. Krogan. A SARS-CoV-2 protein interaction map reveals targets for drug repurposing. *Nature*, apr 2020. ISSN 0028-0836. doi: 10.1038/s41586-020-2286-9.
- Yadi Zhou, Yuan Hou, Jiayu Shen, Yin Huang, William Martin, and Feixiong Cheng. Network-based drug repurposing for novel coronavirus 2019-nCoV/SARS-CoV-2. *Cell discovery*, 6:14, 2020. ISSN 1526-5968. doi: 10.1038/s41421-020-0153-3.
- Susanne Pfefferle, Julia Schöpf, Manfred Kögl, Caroline C. Friedel, Marcel A. Müller, Javier Carbajo-Lozoya, Thorsten Stellberger, Ekatarina von Dall’Armi, Petra Herzog, Stefan Kallies, Daniela Niemeyer, Vanessa Ditt, Thomas Kuri, Roland Züst, Ksenia Pumpor, Rolf Hilgenfeld, Frank Schwarz, Ralf Zimmer, Imke Steffens, Friedemann Weber, Volker Thiel, Georg Herrler, Heinz-Jürgen Thiel, Christel Schwegmann-Wessels, Stefan Pöhlmann, Jürgen Haas, Christian Drosten, and Albrecht von Brunn. The SARS-coronavirus-host interactome: identification of cyclophilins as target for pan-coronavirus inhibitors. *PLoS Pathogens*, 7(10):e1002331, oct 2011. ISSN 1553-7374. doi: 10.1371/journal.ppat.1002331.
- Hugh D. Mitchell, Amie J. Eisfeld, Amy C. Sims, Jason E. McDermott, Melissa M. Matzke, Bobbi-Jo M Webb-Robertson, Susan C. Tilton, Nicolas Tchitchek, Laurence Josset, Chengjun Li, Amy L. Ellis, Jean H. Chang, Robert A. Heegel, Maria L. Luna, Athena A. Schepmoes, Anil K. Shukla, Thomas O. Metz, Gabriele Neumann, Arndt G. Benecke, Richard D. Smith, Ralph S. Baric, Yoshihiro Kawaoka, Michael G. Katze, and Katrina M. Walters. A network integration approach to predict conserved regulators related to pathogenicity of influenza and SARS-CoV respiratory viruses. *PLoS one*, 8(7):e69374, 2013. ISSN 1932-6203. doi: 10.1371/journal.pone.0069374.
- Janick D Stucki, Nina Hobi, Artur Galimov, Andreas O. Stucki, Nicole Schneider-Daum, Claus-Michael Lehr, Hanno Huwer, Manfred Frick, Manuela Funke-Chambour, Thomas Geiser, and Olivier T. Guenat. Medium throughput breathing human primary cell alveolus-on-chip model. *Scientific reports*, 8(1):14359, dec 2018. ISSN 2045-2322. doi: 10.1038/s41598-018-32523-x.
- Adriaan H de Wilde, Eric J Snijder, Marjolien Kikkert, and Martijn J van Hemert. Host Factors in Coronavirus Replication. *Current topics in microbiology and immunology*, 419 (October):1–42, 2012. ISSN 0070-217X. doi: 10.1007/82_2017_25.
- Ritu Kushwaha, Nirmala Jagadish, Manjunath Kustagi, Mark J. Tomishima, Geetu Mendiratta, Mukesh Bansal, Hyunjae R. Kim, Pavel Sumazin, Mariano J. Alvarez, Celine Lefebvre, Patricia Villagrasa-Gonzalez, Agnes Viale, James E. Korkola, Jane Houldsworth, Darren R. Feldman, George J. Bosl, Andrea Califano, and R. S. K. Chaganti. Interrogation of a context-specific transcription factor network identifies novel regulators of pluripotency. *Stem cells (Dayton, Ohio)*, 33(2):367–77, feb 2015. ISSN 1549-4918. doi: 10.1002/stem.1870.
- Celine Lefebvre, Presha Rajbhandari, Mariano J Alvarez, Pradeep Bandaru, Wei Keat Lim, Mai Sato, Kai Wang, Pavel Sumazin, Manjunath Kustagi, Brygida C Bisikirska, Katia Basso, Pedro Beltrao, Nevan Krogan, Jean Gautier, Riccardo Dalla-Favera, and Andrea Califano. A human B-cell interactome identifies MYB and FOXM1 as master regulators of proliferation in germinal centers. *Molecular systems biology*, 6(377):377, jun 2010. ISSN 1744-4292. doi: 10.1038/msb.2010.31.
- Jinsook Son, Hongxu Ding, Domenico Accii, and Andrea Califano. AFF3 and BACH2 are master regulators of metabolic inflexibility, beta/alpha-cell transition, and dedifferentiation in type 2 diabetes. *bioRxiv*, page 768135, sep 2019. doi: 10.1101/768135.
- Andrea Califano and Mariano J Alvarez. The recurrent architecture of tumour initiation, progression and drug sensitivity. *Nature reviews. Cancer*, 17(2):116–130, dec 2017. ISSN 1474-1768. doi: 10.1038/nrc.2016.124.
- Maria Stella Carro, Wei Keat Lim, Mariano Javier Alvarez, Robert J Bollow, Xudong Zhao, Evan Y Snyder, Erik P Sulman, Sandrine L Anne, Fiona Doetsch, Howard Colman, Anna Lasorella, Ken Aldape, Andrea Califano, and Antonio Iavarone. The transcriptional network for mesenchymal transformation of brain tumours. *Nature*, 463(7279):318–25, jan 2010. ISSN 1476-4687. doi: 10.1038/nature08712.
- Presha Rajbhandari, Gonzalo Lopez, Claudia Capdevila, Beatrice Salvatori, Jiyang Yu, Ruth Rodriguez-Barrueco, Daniel Martinez, Mark Yarmarkovich, Nina Weichert-Leahey, Brian J. Abraham, Mariano J. Alvarez, Archana Iyer, Jo Lynne Harenza, Derek Oldridge, Kathleen De Preter, Jan Koster, Shahab Asgharzadeh, Robert C. Seeger, Jun S. Wei, Javed Khan, Jo Vandesompele, Pieter Mestdagh, Rogier Versteeg, A. Thomas Look, Richard A. Young, Antonio Iavarone, Anna Lasorella, Jose M. Silva, John M. Maris, and Andrea Califano. Cross-Cohort Analysis Identifies a TEAD4-MYC Positive Feedback Loop as the Core Regulatory Element of High-Risk Neuroblastoma. *Cancer discovery*, 8(5):582–599, may 2018. ISSN 2159-8290. doi: 10.1158/2159-8290.CD-16-0861.

70. Mercedes Bermejo, María Rosa López-Huertas, Javier García-Pérez, Núria Climent, Benjamin Descours, Juan Ambrosioni, Elena Mateos, Sara Rodríguez-Mora, Lucía Rus-Bercial, Monsef Benkirane, José M Miró, Montserrat Plana, José Alcamí, and Mayte Coiras. Dasa-tinib inhibits HIV-1 replication through the interference of SAMHD1 phosphorylation in CD4+ T cells. *Biochemical pharmacology*, 106:30–45, apr 2016. ISSN 1873-2968. doi: 10.1016/j.bcp.2016.02.002.
71. Szu-Yuan Pu, Fei Xiao, Stanford Schor, Elena Bekerman, Fabio Zanini, Rina Barouch-Bentov, Claude M Nagamine, and Shirir Einav. Feasibility and biological rationale of repurposing sunitinib and erlotinib for dengue treatment. *Antiviral research*, 155:67–75, 2018. ISSN 1872-9096. doi: 10.1016/j.antiviral.2018.05.001.
72. Gregory Neveu, Amotz Ziv-Av, Rina Barouch-Bentov, Elena Berkerman, Jon Mulholland, and Shirir Einav. AP-2-associated protein kinase 1 and cyclin G-associated kinase regulate hepatitis C virus entry and are potential drug targets. *Journal of virology*, 89(8):4387–404, apr 2015. ISSN 1098-5514. doi: 10.1128/JVI.02705-14.
73. Elena Bekerman, Gregory Neveu, Ana Shulla, Jennifer Brannan, Szu-Yuan Pu, Stanley Wang, Fei Xiao, Rina Barouch-Bentov, Russell R. Bakken, Roberto Mateo, Jennifer Govero, Claude M. Nagamine, Michael S. Diamond, Steven De Jonghe, Piet Herdewijn, John M. Dye, Glenn Randall, and Shirir Einav. Anticancer kinase inhibitors impair intracellular viral trafficking and exert broad-spectrum antiviral effects. *The Journal of clinical investigation*, 127(4):1338–1352, apr 2017. ISSN 1558-8238. doi: 10.1172/JCI89857.
74. Yang-Fei Xiang, Chui-Wen Qian, Guo-Wen Xing, Jing Hao, Min Xia, and Yi-Fei Wang. Anti-herpes simplex virus efficacies of 2-aminobenzamide derivatives as novel HSP90 inhibitors. *Bioorganic & medicinal chemistry letters*, 22(14):4703–6, jul 2012. ISSN 1464-3405. doi: 10.1016/j.bmcl.2012.05.079.
75. Abhay P S Rathore, Timothy Haystead, Pratyush K Das, Andres Merits, Mah-Lee Ng, and Subhash G Vasudevan. Chikungunya virus nsP3 & nsP4 interacts with HSP-90 to promote virus replication: HSP-90 inhibitors reduce CHIKV infection and inflammation in vivo. *Antiviral research*, 103:7–16, mar 2014. ISSN 1872-9096. doi: 10.1016/j.antiviral.2013.12.010.
76. Joseph Newman, Amin S Asfor, Stephen Berryman, Terry Jackson, Stephen Curry, and Tobias J Tutthill. The Cellular Chaperone Heat Shock Protein 90 Is Required for Foot-and-Mouth Disease Virus Capsid Precursor Processing and Assembly of Capsid Pentamers. *Journal of virology*, 92(5), 2018. ISSN 1098-5514. doi: 10.1128/JVI.01415-17.
77. Rui Cui, Yizhuo Wang, Liu Wang, Guiming Li, Ke Lan, Ralf Altmeyer, and Gang Zou. Cyclopiazonic acid, an inhibitor of calcium-dependent ATPases with antiviral activity against human respiratory syncytial virus. *Antiviral research*, 132:38–45, 2016. ISSN 1872-9096. doi: 10.1016/j.antiviral.2016.05.010.
78. Aline Schögler, Oliver Caliaro, Melanie Brügger, Blandina I Oliveira Esteves, Izabela Nita, Amiq Gazdhar, Thomas Geiser, and Marco P Alves. Modulation of the unfolded protein response pathway as an antiviral approach in airway epithelial cells. *Antiviral research*, 162:44–50, 2019. ISSN 1872-9096. doi: 10.1016/j.antiviral.2018.12.007.
79. Nan Nwe Win, Tatsuo Kanda, Masato Nakamura, Shingo Nakamoto, Hiroaki Okamoto, Osamu Yokosuka, and Hiroshi Shirasawa. Free fatty acids or high-concentration glucose enhances hepatitis A virus replication in association with a reduction in glucose-regulated protein 78 expression. *Biochemical and biophysical research communications*, 483(1):694–699, 2017. ISSN 1090-2104. doi: 10.1016/j.bbrc.2016.12.080.
80. Karyopharm Therapeutics Inc. Karyopharm Announces Dosing of First Patient in Randomized Study Evaluating Low Dose Selinexor in Patients with Severe COVID-19, 2020.
81. Alexander Dobin, Carrie A. Davis, Felix Schlesinger, Jorg Drenkow, Chris Zaleski, Sonali Jha, Philippe Batut, Mark Chaisson, and Thomas R. Gingeras. STAR: ultrafast universal RNA-seq aligner. *Bioinformatics (Oxford, England)*, 29(1):15–21, jan 2013. ISSN 1367-4811. doi: 10.1093/bioinformatics/bts635.
82. Michael I Love, Wolfgang Huber, and Simon Anders. Moderated estimation of fold change and dispersion for RNA-seq data with DESeq2. *Genome biology*, 15(12):550, 2014. ISSN 1474-760X. doi: 10.1186/s13059-014-0550-8.
83. G K Smyth. Linear models and empirical Bayes methods for assessing differential expression in microarray experiments. *Statistical Applications in Genetics and Molecular Biology*, 3(1):Art3, 2004.

Methods

Cell lines. NCI-H1793 cells were obtained from ATCC (CRL-5896), mycoplasma tested and maintained in DMEM:F12 medium supplemented with 5 $\mu\text{g/ml}$ insulin, 10 $\mu\text{g/ml}$ transferrin, 30 nM sodium selenite, 10 nM β -estradiol, 4.5 mM L-glutamine and 5% fetal bovine serum. Cells were grown in a humidified incubator at 37°C and 5% CO₂.

Lung epithelium context-specific drug mechanism of action database. The drug-perturbation dataset was generated as follows. First, the ED_{20} for each of the 133 FDA-approved drugs and 195 investigational compounds in oncology was estimated in NCI-H1793 cells by performing 10-point dose-response curves in triplicate, using total ATP content as read-out. Briefly, 2,000 cells per well were plated in 384-well plates. Small-molecule compounds were added with a 96-well pin-tool head 12h after cell plating. Viable cells were quantified 48h later by ATP assay (CellTiterGlo,

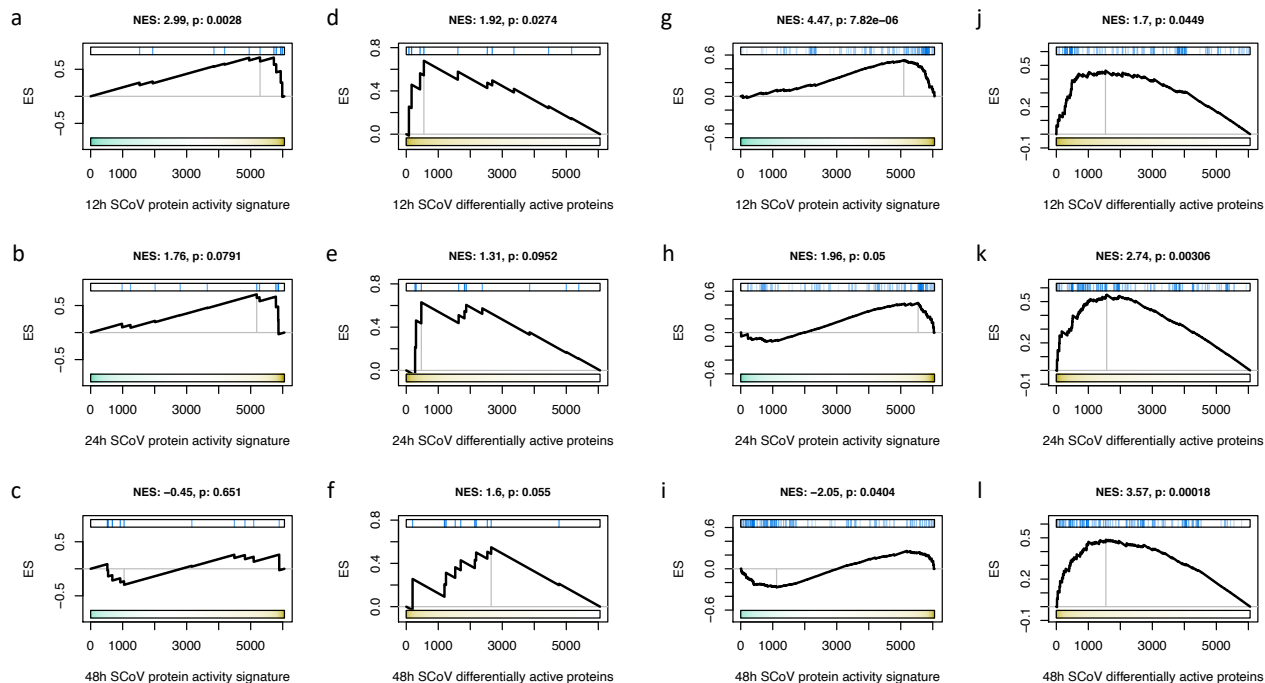
Promega). Relative cell viability was computed using matched DMSO control wells as reference. ED_{20} was estimated by fitting a four-parameter sigmoid model to the titration results. NCI-H1793 cells, plated in 384-well plates, were then perturbed with a library of 328 FDA-approved drugs and small-molecule compounds at their corresponding ED_{20} concentration. Cells were lysed at 24h after small-molecule compound perturbation and the transcriptome was profiled by PLATE-Seq(55). RNA-Seq reads were mapped to the human reference genome assembly 38 using the STAR aligner(81). Expression data were then normalized by equivariance transformation, based on the negative binomial distribution with the DESeq R-system package (Bioconductor(82)). At least two replicates for each condition were obtained. Differential gene expression signatures were computed by comparing each condition with plate-matched vehicle control samples using a moderated Student’s t-test as implemented in the limma package from Bioconductor(83). Individual gene expression signatures were then transformed into protein activity signatures with the VIPER algorithm(37), based on the a lung adenocarcinoma context-specific regulatory network available from the aracne.networks package from Bioconductor.

Computational analysis. Enrichment of gene-sets for biological hallmarks was performed using Gene Set Enrichment Analysis(52) with the Molecular Signatures Database MSigDB v7.1(53). Enrichment analysis for virus-interacting host proteins (PPI) on SARS-CoV induced protein activity signatures, as well as the OncoMatch(56) analysis to assess the conservation of the virus-induced MR protein activity on NCI-H1793 lung adenocarcinoma cells were performed with the aREA algorithm(37).

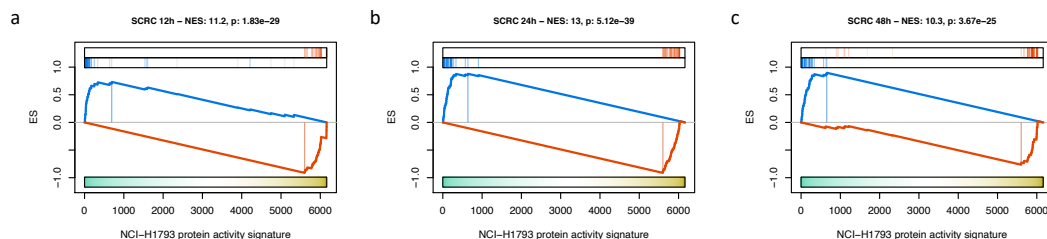
ViroTreat analysis. ViroTreat was performed by computing the enrichment of the top/bottom 50 most differentially active proteins in response to drug perturbation—the context-specific mechanism of action—on the virus-induced protein activity signature using the aREA algorithm(37). P-values for significantly negative enrichment were estimated using 1-tail aREA analysis, and multiple hypothesis testing was controlled by the Bonferroni’s correction.

Code availability. All the code used in this work is freely available for research purposes. VIPER and aREA algorithms are part of the “viper” R-system’s package available from Bioconductor. The lung adenocarcinoma context-specific interactome is available as part of the “aracne.networks” R-system’s package from Bioconductor.

Supplementary Figures and Tables



Supplementary Figure 1. Enrichment of SARS-CoV- and SARS-CoV2-interacting host proteins among the most differentially active proteins after SARS-CoV infection. (a–f) Enrichment of 12 SARS-CoV-interacting host proteins, or (g–l) 89 SARS-CoV2-interacting proteins on SARS-CoV induced protein activity signatures at 12h (a, d, g and j), 24h (b, e, h and k) and 48h (c, f, i and l) after infection. GSEA plots show the enrichment score (y-axis) and the SARS-CoV induced protein activity signature (x-axis), where 6,054 regulatory proteins were rank-sorted from the one showing the strongest inactivation (left) to the one showing the strongest activation (right) in response to SARS-CoV infection (a–c and g–i); or where the regulatory proteins were sorted from the most differentially active (left) to the least differentially active (right) after SARS-CoV infection. NES and *p*-value were estimated by 2-tail aREA test and shown on top of each plot.



Supplementary Figure 2. Conservation of the SARS-CoV induced checkpoint in NCI-H1793 cells. GSEA plots for the enrichment of the top 25 most activated proteins (red vertical lines), and top 25 most inactivated proteins (blue vertical lines) by SARS-CoV infection at 12h (a), 24h (b) and 48h (c) after infection. The x-axis shows 6,054 proteins rank-sorted from the most inactivated ones (left) to the most activated ones (right) in NCI-H1793 cells when compared against 86 non-small cell lung cancer cell lines. The y-axis shows the GSEA enrichment score. NES and *p*-value, estimated by 2-tail aREA test, are indicated on top of each plot.

GeneID	Symbol	NES			p-value, Bonferroni's corrected			Description
		12h	24h	48h	12h	24h	48h	
3659	IRF1	0.9	3.11	7.04	1	1	1.17E-08	interferon regulatory factor 1
23764	MAFF	3.11	3.03	7.03	1	1	1.22E-08	MAF bZIP transcription factor F
1843	DUSP1	4.47	3.82	6.96	0.0483	0.806	2.02E-08	dual specificity phosphatase 1
567	B2M	0.6	2.78	6.94	1	1	2.41E-08	beta-2-microglobulin
80833	APOL3	-0.38	3.11	6.91	1	1	2.85E-08	apolipoprotein L3
282618	IL29	2.66	4.75	6.91	1	0.012	2.92E-08	interferon lambda 1
1839	HBEFG	2.68	4.12	6.9	1	0.233	3.11E-08	heparin binding EGF like growth factor
3726	JUNB	4.46	4.77	6.9	0.0503	0.0113	3.25E-08	JunB proto-oncogene, AP-1 transcription factor subunit
7538	ZFP36	4.69	3.96	6.84	0.0164	0.447	4.70E-08	ZFP36 ring finger protein
8542	APOL1	0.57	3.05	6.75	1	1	8.96E-08	apolipoprotein L1
4061	LY6E	3.27	5.23	6.65	1	0.00101	1.81E-07	lymphocyte antigen 6 family member E
8767	RIPK2	3.32	5.85	6.64	1	3.01E-05	1.86E-07	receptor interacting serine/threonine kinase 2
3717	JAK2	0.65	1.87	6.54	1	1	3.73E-07	Janus kinase 2
93594	WDR67	3.16	5.74	6.46	1	5.72E-05	6.34E-07	TBC1 domain family member 31
4149	MAX	0.95	2.78	6.42	1	1	8.39E-07	MYC associated factor X
80149	ZC3H12A	1.53	2.9	6.4	1	1	9.32E-07	zinc finger CCCH-type containing 12A
9510	ADAMTS1	3.27	4.12	6.3	1	0.228	1.76E-06	ADAM metalloproteinase with thrombospondin type 1 motif 1
467	ATF3	3.07	3.28	6.27	1	1	2.17E-06	activating transcription factor 3
4277	MICB	2.87	5.72	6.22	1	6.30E-05	3.08E-06	MHC class I polypeptide-related sequence B
29126	CD274	0.01	3.38	6.05	1	1	8.79E-06	CD274 molecule
1408	CRY2	-6.05	-12.15	-11.68	8.69E-06	3.53E-30	9.94E-28	cryptochrome circadian regulator 2
7508	XPC	-6.06	-8.95	-7.66	8.19E-06	2.09E-15	1.14E-10	XPC complex subunit, DNA damage recognition and repair factor
2796	GNRH1	-6.09	-6.21	-3.95	6.77E-06	3.22E-06	0.463	gonadotropin releasing hormone 1
7569	ZNF182	-6.19	-5.78	-2.29	3.64E-06	4.47E-05	1	zinc finger protein 182
117608	ZNF354B	-6.22	-6.33	-3.12	3.08E-06	1.46E-06	1	zinc finger protein 354B
10608	MXD4	-6.22	-10.81	-8.9	2.92E-06	1.92E-23	3.33E-15	MAX dimerization protein 4
152098	ZCWPW2	-6.33	-11.48	-9.5	1.45E-06	1.04E-26	1.23E-17	zinc finger CW-type and PWWP domain containing 2
26118	WSB1	-6.46	-5.8	-3.23	6.52E-07	4.12E-05	1	WD repeat and SOCS box containing 1
2550	GABBR1	-6.47	-6.13	-4	5.88E-07	5.43E-06	0.391	gamma-aminobutyric acid type B receptor subunit 1
84163	GTF2IRD2	-6.57	-10.34	-8.55	3.14E-07	2.95E-21	7.16E-14	GTF2I repeat domain containing 2
11030	RBPMS	-6.8	-10.64	-10.7	6.32E-08	1.22E-22	6.46E-23	RNA binding protein, mRNA processing factor
29800	ZDHHC1	-7.21	-10.58	-10.03	3.39E-09	2.17E-22	6.51E-20	zinc finger DHHC-type containing 1
58487	CREBZF	-7.26	-6.76	-3.87	2.35E-09	8.36E-08	0.669	CREB/ATF bZIP transcription factor
80778	ZNF34	-2.47	-6.09	-4.84	1	6.87E-06	0.0078	zinc finger protein 34
7626	ZNF75D	-4.64	-6.11	-3.13	0.0208	6.13E-06	1	zinc finger protein 75D
58191	CXCL16	-3.97	-6.16	-5.28	0.44	4.46E-06	0.000802	C-X-C motif chemokine ligand 16
6604	SMARCD3	-3.62	-6.21	-5.57	1	3.31E-06	0.000156	SWI/SNF related, matrix associated, actin dependent regulator of chromatin, subfamily d, member 3
23286	WWC1	-3.76	-6.32	-6.38	1	1.62E-06	1.10E-06	WW and C2 domain containing 1
9278	ZBTB22	-4.48	-6.62	-6.81	0.0442	2.12E-07	5.84E-08	zinc finger and BTB domain containing 22
9912	ARHGAP44	-4.86	-6.69	-6.19	0.0071	1.35E-07	3.60E-06	Rho GTPase activating protein 44
975	CD81	-4.5	-6.75	-5.42	0.0416	8.95E-08	0.000359	CD81 molecule
7113	TMPRSS2	-3.19	-6.81	-6.73	1	5.84E-08	1.02E-07	transmembrane serine protease 2
55625	ZDHHC7	-2.46	-6.93	-7.07	1	2.55E-08	9.64E-09	zinc finger DHHC-type palmitoyltransferase 7
23492	CBX7	-5	-6.94	-7	0.00342	2.40E-08	1.52E-08	chromobox 7
23221	RHOBTB2	-3.83	-6.96	-6.75	0.768	2.06E-08	9.13E-08	Rho related BTB domain containing 2
728656	DMRTC1B	-4.82	-6.98	-5.51	0.00857	1.80E-08	0.000215	DMRT like family C1B
2122	MECOM	-5.02	-6.98	-7.22	0.00313	1.74E-08	3.26E-09	MDS1 and EVI1 complex locus
163255	ZNF540	-5.07	-6.99	-4.62	0.00235	1.63E-08	0.0237	zinc finger protein 540
5333	PLCD1	-5.21	-7.03	-7.04	0.00113	1.24E-08	1.12E-08	phospholipase C delta 1
57326	PBXIP1	-2.97	-7.08	-6.81	1	8.66E-09	6.10E-08	PBX homeobox interacting protein 1
81550	TDRD3	-4.06	-7.32	-6.28	0.297	1.50E-09	2.00E-06	tudor domain containing 3
10206	TRIM13	-2.34	-7.44	-7.36	1	6.24E-10	1.08E-09	tripartite motif containing 13
63976	PRDM16	-3.38	-7.57	-6.82	1	2.24E-10	5.48E-08	PR/SET domain 16
4784	NFIX	-4.25	-7.6	-7.36	0.131	1.84E-10	1.15E-09	nuclear factor I X
2788	NGF7	-5.96	-7.74	-7.26	1.57E-05	6.01E-11	2.28E-09	G protein subunit gamma 7
284390	ZNF763	-5.99	-8.49	-7.99	1.26E-05	1.24E-13	8.33E-12	zinc finger protein 763
4306	NR3C2	-3.95	-9.12	-9.09	0.464	4.65E-16	6.10E-16	nuclear receptor subfamily 3 group C member 2
5934	RBL2	-5.74	-9.31	-8.23	5.80E-05	7.70E-17	1.16E-12	RB transcriptional corepressor like 2
202018	TAPT1	-4.45	-9.33	-7.81	0.0521	6.47E-17	3.53E-11	transmembrane anterior posterior transformation 1
389524	GTF2IRD2B	-5.5	-9.51	-8.96	0.000234	1.14E-17	1.88E-15	GTF2I repeat domain containing 2B
54386	TERF2IP	-3.95	-9.6	-8.99	0.467	4.90E-18	1.47E-15	TERF2 interacting protein
6778	STAT6	-5.67	-9.77	-7.97	8.80E-05	8.75E-19	9.42E-12	signal transducer and activator of transcription 6
7008	TEF	-5.26	-10.43	-9.75	0.000857	1.13E-21	1.09E-18	TEF transcription factor, PAR bZIP family member
7067	THRA	-5.28	-10.82	-9.83	0.00079	1.70E-23	5.22E-19	thyroid hormone receptor alpha
80108	ZFP2	-5.76	-11.16	-10.64	4.99E-05	3.73E-25	1.21E-22	ZFP2 zinc finger protein
57659	ZBTB4	-5.67	-11.46	-11.14	8.65E-05	1.27E-26	4.71E-25	zinc finger and BTB domain containing 4

Supplementary Table 2. FDA-approved drugs and late-stage (phase 2 and 3) investigational compounds in oncology covered by the lung epithelium context-specific MoA database. The table lists the drug/compound name, concentration used to perturb NCI-H1793 lung adenocarcinoma cells, FDA-approval status known primary targets.

Compound	Concentration	FDA-approved	Known targets
Acalabrutinib	1.9 μ M	Yes	BTK
Afatinib	187 nM	Yes	EGFR, ERBB2
Albendazole	900 nM	Yes	
Alectinib	1 μ M	Yes	ALK
Alexidine	1 μ M	Yes	PTPMT1
Alpelisib	370 nM	Yes	PIK3CA, PIK3CB, PIK3CD, PIK3CG
Aminopterin	1.1 μ M	Yes	
Amsacrine	2.4 μ M	Yes	
AP26113	3.8 μ M	Yes	ALK, EGFR
Apremilast	450 nM	Yes	
Arsenic trioxide	400 nM	Yes	TXNRD1, PML
Axitinib	144 nM	Yes	FLT1, FLT4, KDR
Azacitidine	4.1 μ M	Yes	DNMT1, DNMT3A
Belinostat	2.5 μ M	Yes	pan-HDAC
Benzethonium chloride	5 μ M	Yes	
Bexarotene	1.6 μ M	Yes	RXRA, RXRB, RXRG
Bleomycin	276 nM	Yes	LIG1, LIG3
Bortezomib	68 nM	Yes	Proteasome
Bosentan	833 nM	Yes	EDNRA, EDNRB
Bosutinib	377 nM	Yes	ABL1, SRC
Busulfan	296 nM	Yes	
Cabazitaxel	3 nM	Yes	Tubulin
Cabergoline	0 pM	Yes	
Cabozantinib	1.1 μ M	Yes	KDR, RET, MET
Calcitriol	5 nM	Yes	
Carboplatin	1 μ M	Yes	
Carfilzomib	24 nM	Yes	Proteasome
Carmustine	1.6 μ M	Yes	GSR
Ceritinib	1.4 μ M	Yes	ALK
Cetylpyridinium Chloride	3 μ M	Yes	
Cinacalcet	2.4 μ M	Yes	
Cladribine	718 nM	Yes	
Clarithromycin	1 μ M	Yes	
Clofarabine	437 nM	Yes	
Clofoctol	4.5 μ M	Yes	
Cobimetinib	514 nM	Yes	MAP2K1
Copanlisib	674 nM	Yes	PIK3CA, PIK3CB, PIK3CD, PIK3CG
Crizotinib	193 nM	Yes	MET, ALK
Cyclosporine	1.9 μ M	Yes	
Dabrafenib	1.6 μ M	Yes	BRAF, RAF1
Dacomitinib	53 nM	Yes	EGFR, ERBB2
Dactinomycin	3 nM	Yes	TOP2A, TOP2B
Dasatinib	345 nM	Yes	SRC, ABL1, BCR, KIT
Daunorubicin	134 nM	Yes	TOP2A, TOP2B
Decitabine	644 nM	Yes	DNMT1, DNMT3A
Digoxigenin	285 nM	Yes	
Disulfiram	14 nM	Yes	ALDH2, DBH
Domiphen Bromide	2.5 μ M	Yes	
Doxorubicin	239 nM	Yes	TOP2A
Dronedarone	2 μ M	Yes	
Enasidenib	1.9 μ M	Yes	IDH2, IDH1
Epigallocatechin	436 nM	Yes	
Epirubicin	162 nM	Yes	TOP2A, CHD1
Erlotinib	3.4 μ M	Yes	EGFR
Estramustine	3.9 μ M	Yes	
Etoposide	2 μ M	Yes	TOP2A, TOP2B
Everolimus	84 nM	Yes	MTOR
Exemestane	1.5 μ M	Yes	CYP19A1
Fedratinib	1.5 μ M	Yes	
Fludarabine	209 nM	Yes	POLA1, RRM1, RRM2
Fulvestrant	32 nM	Yes	ESR1, ESR2
Gefitinib	571 nM	Yes	EGFR
Gemcitabine	316 nM	Yes	TYMS
Gentian Violet	45 nM	Yes	
Homoharringtonine	9 nM	Yes	
Hydroxychloroquine	434 nM	Yes	
Ibrutinib	354 nM	Yes	BTK
Idarubicin	24 nM	Yes	TOP2A
Idelalisib	1 μ M	Yes	PIK3CD, PIK3CA, PIK3CB, PIK3CG
Irinotecan	2.9 μ M	Yes	TOP1
Ixabepilone	153 pM	Yes	Tubulin
Ixazomib	43 nM	Yes	PSMB5
Lanatoside	65 nM	Yes	
Lenalidomide	1.7 μ M	Yes	TNF, TNFSF11
Lenvatinib	647 nM	Yes	FLT4, KDR, FLT1
Letrozole	1.9 μ M	Yes	CYP19A1
Leucovorin	2.1 μ M	Yes	
Leuprolide	76 nM	Yes	GNRHR

Compound	Concentration	FDA-approved	Known targets
Mechlorethamine	883 nM	Yes	
Megestrol acetate	49 nM	Yes	
Melphalan	819 nM	Yes	
Mercaptopurine	867 nM	Yes	
Miconazole	2.5 μ M	Yes	
Midostaurin	700 nM	Yes	FLT3, PRKCA
Mitomycin	4.2 μ M	Yes	
Mitoxantrone	62 nM	Yes	TOP2A
Mycophenolate mofetil	1.8 μ M	Yes	IMPDH1, IMPDH2
Nebivolol	2.7 μ M	Yes	ADRB1
Neratinib	230 nM	Yes	ERBB2, EGFR
Niclosamide	500 nM	Yes	
Nilotinib	2.3 μ M	Yes	ABL1, BCR, PDGFRA, PDGFRB
Nintedanib	139 nM	Yes	FLT4, KDR, PDGFRA, PDGFRB, FGFR1, FGFR2, FLT1
Octreotide	5 nM	Yes	SSTR2, SSTR3, SSTR5
Osimertinib	1.7 μ M	Yes	EGFR
Oxaliplatin	2.7 μ M	Yes	
Palbociclib	115 nM	Yes	CDK4, CDK6
Panobinostat	45 nM	Yes	pan-HDAC
Penfluridol	1 μ M	Yes	
Pentostatin	1 μ M	Yes	ADA
Phenelzine	1.3 μ M	Yes	MAOA, MAOB
Pimozide	3 μ M	Yes	DRD3, DRD2
Pomalidomide	212 nM	Yes	TNF
Ponatinib	80 nM	Yes	ABL1, BCR, FGFR1, KDR, FLT1, TEK, FLT3, FGFR2, FGFR3, FGFR4
Pralatrexate	64 nM	Yes	DHFR, TYMS
Prednisone	845 nM	Yes	
Procarbazine	2.3 μ M	Yes	MAOB, MAOA
Propranolol	1.6 μ M	Yes	ADRB1
Raloxifene	9 nM	Yes	ESR1
Romidepsin	697 nM	Yes	pan-HDAC
Rosiglitazone	2.2 μ M	Yes	
Rucaparib	3.2 μ M	Yes	PARP1, PARP2, PARP3
Selinexor	137 nM	Yes	XPO1
Sorafenib	4.9 μ M	Yes	RAF1, BRAF, KDR, PDGFRB
Sunitinib	49 nM	Yes	KIT, PDGFRB, KDR, FLT3
Tacrolimus	5 μ M	Yes	
Talazoparib	61 nM	Yes	PARP2
Tamoxifen	1.1 μ M	Yes	ESR1
Temsirolimus	81 nM	Yes	MTOR
Teniposide	212 nM	Yes	TOP2A, TOP2B
Thioguanine	871 nM	Yes	DNMT1
Thiotepa	3.6 μ M	Yes	
Tofacitinib	309 nM	Yes	JAK3, JAK1, STAT3
Topotecan	162 nM	Yes	TOP1
Toremifene	1.6 μ M	Yes	ESR1
Trametinib	36 nM	Yes	MAP2K1, MAP2K2
Valproic Acid	2.4 μ M	Yes	HDAC9
Vemurafenib	1 nM	Yes	BRAF, RAF1
Verteporfin	2 μ M	Yes	
Vinblastine	222 nM	Yes	Tubulin
Vinorelbine	2 nM	Yes	Tubulin
Vitamin A	2.1 μ M	Yes	
Vorinostat	1.4 μ M	Yes	pan-HDAC
Zinc Pyrithione	500 nM	Yes	
10-DEBC	3.9 μ M	No	AKT1, AKT2, AKT3
2,3-DCPE	3.5 μ M	No	
7-Desacetoxy-6,7-dehydrogedunin	2 μ M	No	
Abexinostat	339 nM	No	HDAC1, HDAC8
ABT-751	5 μ M	No	
AC-93253	190 nM	No	
AEE788	175 nM	No	ERBB2, KDR, EGFR
Akt Inhibitor IV	255 nM	No	AKT1, AKT2, AKT3
Alisertib	1.1 μ M	No	AURKA
AMG-208	2.7 μ M	No	MET
AMG-900	2.5 μ M	No	AURKA, AURKB, AURKC
Amuvatinib	24 nM	No	KIT, FLT3, MET, RET, PDGFRA, RAD51
AP1903	903 nM	No	
AT9283	936 nM	No	JAK2, JAK3, AURKA, AURKB
Atrasentan	1.7 μ M	No	EDNRA
AVN-944	3.7 μ M	No	
AZD1480	131 nM	No	JAK2
AZD1775	156 nM	No	WEE1
AZD5363	1.6 μ M	No	AKT1, AKT2, AKT3
Bardoxolone Methyl	145 nM	No	CHUK, IKBKB, NFKB1, NFKB2, NFE2L2, NFKBIA
Baricitinib	415 nM	No	JAK1, JAK2, TYK2
Bax channel blocker	2.5 μ M	No	BAX
BAY 11-7082	5 μ M	No	
Bay 11-7085	15 nM	No	IKKB
Bay 11-7821	5 μ M	No	NFKBIA
BI 2536	250 nM	No	
BI-78D3	3 μ M	No	MAPK8
BI-87G3	3.5 μ M	No	MAPK8
Binimetinib	1 μ M	No	MAP2K2, MAP2K1

Compound	Concentration	FDA-approved	Known targets
Birinapant	5 μ M	No	BIRC2, XIAP
BMS-833923	1.1 μ M	No	
Buparlisib	300 nM	No	PIK3CA
Calcimycin	340 nM	No	
Calmidazolium	500 nM	No	CALM1
Camptothecin	4 nM	No	
Canertinib	640 nM	No	EGFR, ERBB2, ERBB4
CC-223	931 nM	No	MTOR
Cediranib	222 nM	No	FLT4, KDR, FLT1, KIT, PDGFRA, CSF1R, FLT3, PDGFRB
CGP-71683	1.3 μ M	No	NPY5R
Chlorothalonil	3.9 μ M	No	
Combretastatin A4	1 μ M	No	Tubulin
CP-100356	3.5 μ M	No	ABCB1
Crenolanib	149 nM	No	PDGFRA, PDGFRB, CSF1R, FLT3, KIT
Cyproterone	166 nM	No	
Dacinostat	145 nM	No	HDAC1
Diallyl trisulfide	880 nM	No	
Dinaciclib	4 nM	No	CDK2, CDK5, CDK1, CDK9
Dovitinib	591 nM	No	FGFR3, FLT3, KIT, FGFR1, FLT1, PDGFRA, PDGFRB
Elesclomol	54 nM	No	
Eniluracil	4 μ M	No	
ENMD-2076	1.5 μ M	No	
Entinostat	1.7 μ M	No	HDAC1, HDAC3, HDAC2, HDAC9
Entospletinib	1.4 μ M	No	SYK
Enzastaurin	2.2 μ M	No	
Epothilone B	251 nM	No	
Epothilone D	1 μ M	No	
EPZ-6438	2.4 μ M	No	EZH2
ER-27319	1.5 μ M	No	SYK
Evans blue	500 nM	No	
Ezatiostat	2.5 μ M	No	GSTP1
Flavopiridol	90 nM	No	CDK1, CDK2, CDK4, CDK6
Fluspirilene	5 μ M	No	
Foretinib	116 nM	No	MET, KDR
Galeterone	3.6 μ M	No	
Galunisertib	2.7 μ M	No	TGFBR1
Gambogic acid	425 nM	No	
GBR-12909	2.5 μ M	No	
Gedatolisib	12 nM	No	PIK3CA, PIK3CG, MTOR
Gilteritinib	2.3 μ M	No	FLT3
Gitoxigenin diacetate	70 nM	No	
Givinostat	235 nM	No	pan-HDAC
Go6976	3 μ M	No	PRKCA, PRKCB, PRKCG, PRKCD
Gossypol	2.4 μ M	No	BCL2, BCL2L1
GSK-3 inhibitor IX	3.5 μ M	No	GSK3A, GSK3B
GSK1059615	2 μ M	No	
GSK461364	514 nM	No	PLK1
GW-843682X	1 μ M	No	PLK1, PLK3
Halofuginone	1 nM	No	
HMN-214	515 nM	No	
Homidium bromide	3.3 μ M	No	
IKK-16	2.2 μ M	No	CHUK, IKKBK
IMD0354	500 nM	No	
INCA-6	2.3 μ M	No	NFATC2, NFATC1
INK-128	17 nM	No	MTOR
Ipatasertib	459 nM	No	AKT1, AKT3, AKT2
Ispinesib	543 nM	No	
JTC-801	2 μ M	No	
Ki8751	5 μ M	No	KDR
Kinetin riboside	4.9 μ M	No	
Leelamine	2 μ M	No	
Lexibulin	354 nM	No	
Linifanib	1.4 μ M	No	FLT1, FLT3, KDR, PDGFRA, PDGFRB
Luminespib	1.1 μ M	No	HSP90AA1, HSP90AB1
LY-2183240	900 nM	No	FAAH
LY2228820	3 μ M	No	
LY2603618	4.6 μ M	No	
LY2835219	473 nM	No	
LY3023414	87 nM	No	MTOR
Mangostin	500 nM	No	
Methyl 2,5-dihydroxycinnamate	864 nM	No	
MGCD-265	1.1 μ M	No	FLT1, FLT4, KDR, MET, MST1R, TEK
MK-2206	756 nM	No	AKT1, AKT2, AKT3
Mocetinostat	391 nM	No	HDAC1
Momelotinib	1.6 μ M	No	JAK1, JAK2
Motesanib	1.3 μ M	No	FLT1, KDR, FLT4, PDGFRA, PDGFRB, KIT, RET
MST-312	4 μ M	No	TERT
Navitoclax	460 nM	No	BCL2, BCL2L1, BCL2L2
NH125	1.5 μ M	No	EEF2
Niguldipine	2.7 μ M	No	ADRA1A
NSC-95397	2.5 μ M	No	CDC25A, CDC25C, CDC25B
Obatoclax mesylate	145 nM	No	BCL2
Onalespib	4.4 μ M	No	
ONO-4059	2.2 μ M	No	BTK

Compound	Concentration	FDA-approved	Known targets
Oprozomib	380 nM	No	
OTX015	3.9 μ M	No	
P276-00	444 nM	No	
Pacritinib	573 nM	No	JAK2
Pararosaniline	355 nM	No	
PD-166285	75 nM	No	SRC, FGFR1, PDGFRB
PD0325901	667 nM	No	MAP2K1
Perifosine	5 μ M	No	MAPK1, AKT1
Pevonedistat	2.7 μ M	No	NAE1
PF-04691502	147 nM	No	PIK3CA, PIK3CB, PIK3CD, PIK3CG, MTOR
Phenylmercury	435 nM	No	
PI-103	110 nM	No	
PI3KA Inhibitor IV	1 μ M	No	PIK3CA
Picoplatin	2.2 μ M	No	
Pictilisib	599 nM	No	PIK3CA, PIK3CD
Pimasertib	911 nM	No	MAP2K1, MAP2K2
Pirarubicin	8 nM	No	
Plicamycin	182 nM	No	
Plinabulin	1.6 μ M	No	Tubulin
Plumbagin	2 μ M	No	
PP-121	350 nM	No	
Pracinostat	420 nM	No	HDAC3, HDAC1, HDAC2, HDAC6
Prenylamine	2.5 μ M	No	
Prinomastat	468 nM	No	MMP2, MMP9, MMP13, MMP14
Pristimerin	855 nM	No	MGLL
Proscillaridin A	5 nM	No	
Puromycin	1 μ M	No	
PX-12	3 μ M	No	TXN
Pyrvinium	270 nM	No	
Quizartinib	577 nM	No	
RAF265	4.9 μ M	No	
Raltitrexed	11 nM	No	TYMS
Refametinib	2.3 μ M	No	MAP2K1, MAP2K2
Resminostat	4.4 μ M	No	
Rigosertib	90 nM	No	PLK1
Ro 31-8220 Mesylate	2 μ M	No	
RO4929097	1.1 μ M	No	
Rocilinostat	1.5 μ M	No	HDAC6
RS-17053	2.9 μ M	No	ADRA1A
Ryuvidine	3.6 μ M	No	SETD8
Sanguinarine	1 μ M	No	
Sappanone A dimethyl ether	2.4 μ M	No	
Saracatinib	1.1 μ M	No	SRC, ABL1
Satraplatin	1.7 μ M	No	
SB-216641	4 μ M	No	HTR1B
SB-224289	1 μ M	No	HTR1B
SB-743921	250 nM	No	
SCIO-469	4.8 μ M	No	MAPK14
Serdemetan	156 nM	No	
SGL-1776	4 μ M	No	PIM1, PIM2, PIM3
SNX-2112	287 nM	No	HSP90AA1, HSP90AB1
Sphingosine	3 μ M	No	
SRT1720	1.5 μ M	No	
Sulconazole Nitrate	3.1 μ M	No	
Suloctidil	1.5 μ M	No	
Tacedinaline	1.1 μ M	No	HDAC1, HDAC2, HDAC3
TAE684	5 μ M	No	ALK
TAK-733	268 nM	No	MAP2K1
Talampanel	1.1 μ M	No	
Tandutinib	1 μ M	No	FLT3, KIT, PDGFRB
Tariquidar	1.9 μ M	No	ABCB1
Tasquinimod	520 nM	No	S100A9
Telatinib	2.4 μ M	No	FLT4, KIT, KDR
Terfenadine	2.5 μ M	No	HRH1
Thapsigargin	15 nM	No	
Thymoquinone	988 nM	No	
Tivantinib	227 nM	No	MET
Tivozanib	176 nM	No	FLT4, KDR, FLT1
Totanol	4.3 μ M	No	
Trichostatin A	120 nM	No	
Triciribine	782 nM	No	AKT1, AKT2, AKT3
Tyrothricin	210 nM	No	
UCN-01	74 nM	No	AKT1, CHEK1, PDK1, PRKCA, PRKCB
Valinomycin	200 pM	No	
Vatalanib	119 nM	No	KDR, FLT1
Vindesine	23 nM	No	Tubulin
Vistusertib	108 nM	No	MTOR, PIK3CA, PIK3CB, PIK3CD, PIK3CG
Volasertib	1.3 μ M	No	PLK1
Voreloxin	1.2 μ M	No	
Voxtalisisib	504 nM	No	PIK3CG, MTOR, PRKDC
YM155	16 nM	No	BIRC5
Zibotentan	1.7 μ M	No	

Supplementary Table 3. FDA-approved drugs and investigational compounds identified by ViroTreat as significantly inverting the SARS-CoV ViroCheckpoint ($p < 10^{-10}$, BC, 1-tail aREA test). The drugs/compounds were sorted according to ViroTreat-inferred statistical significance as inverters of SARS-CoV 12h-, 24h- and 48h-ViroCheckpoints. The table lists the drug/compound name, FDA-approval status, concentration used to perturb the NCI-H1793 lung adenocarcinoma cells, ViroTreat-estimated statistical significance—expressed as $-\log_{10}(p\text{-value})$ —and know primary targets.

Compound	FDA-approved	Concentration	12	24	48	Known targets
PD0325901	No	667 nM	19.77	27.24	15.92	MAP2K1
Palbociclib	Yes	115 nM	18.49	23.5	15.76	CDK4, CDK6
Resminostat	No	4.4 uM	18.43	18.86	6.31	HDAC1, HDAC3, HDAC6
TAK-733	No	268 nM	17.61	25.3	9.02	MAP2K1
Pimasertib	No	911 nM	16.81	25.61	21.72	MAP2K1, MAP2K2
Selinexor	Yes	137 nM	16.19	19.74	6.44	XPO1
Trametinib	Yes	36 nM	16.01	24.88	14.84	MAP2K1, MAP2K2
PI3KA Inhibitor IV	No	1 uM	15.48	21.12	9.93	PIK3CA
Cobimetinib	Yes	514 nM	14.47	20.61	3.23	MAP2K1
Niclosamide	Yes	500 nM	14.35	15.26	1.18	
Panobinostat	Yes	45 nM	14.33	16.71	3.8	pan-HDAC
Pictilisib	No	599 nM	14.1	10.77	0	PIK3CA, PIK3CD
Dasatinib	Yes	345 nM	14.09	13.58	0.8	SRC, ABL1, BCR, KIT
CC-223	No	931 nM	13.81	7.52	0	MTOR
Everolimus	Yes	84 nM	13.8	8.91	0	MTOR
Foretinib	No	116 nM	13.15	2.41	0	MET, KDR
PF-04691502	No	147 nM	12.61	13.92	8.62	PIK3CA, PIK3CB, PIK3CD, PIK3CG, MTOR
PI-103	No	110 nM	12.46	17.81	7.79	PIK3CA, PIK3CB, PIK3CD, PIK3CG
Refametinib	No	2.3 uM	12.45	19.13	11.13	MAP2K1, MAP2K2
Belinostat	Yes	2.5 uM	12.17	7.44	0	pan-HDAC
Rocilinostat	No	1.5 uM	12.14	5.36	0	HDAC6
UCN-01	No	74 nM	12.06	17.89	11.75	AKT1, CHEK1, PDK1, PRKCA, PRKCB
Motesanib	No	1.3 uM	11.51	8.84	0	FLT1, KDR, FLT4, PDGFRA, PDGFRB, KIT, RET
Erlotinib	Yes	3.4 uM	11.49	9.2	1.32	EGFR
LY3023414	No	87 nM	11.43	4.18	0	MTOR
Thioguanine	Yes	871 nM	11.15	1.71	0	DNMT1
Carfilzomib	Yes	24 nM	10.94	19.4	5.87	Proteasome
Temsirolimus	Yes	81 nM	10.9	7.88	0	MTOR
Bardoxolone Methyl	No	145 nM	10.41	17.55	8.63	CHUK, IKKB, NFKB1, NFKB2, NFE2L2, NFKBIA
IMD0354	No	500 nM	10.24	2.21	0	IKKB
TAE684	No	5 uM	8.81	23.29	24.23	ALK
Thapsigargin	No	15 nM	8.23	21.32	19.56	
AP26113	Yes	3.8 uM	5.93	19.54	18.69	ALK, EGFR
Ki8751	No	5 uM	9.69	19.46	7.52	KDR
Binimetinib	No	1 uM	7.56	17.67	13.27	MAP2K2, MAP2K1
Dovitinib	No	591 nM	7.98	17.39	19.49	FGFR3, FLT3, KIT, FGFR1, FLT1, PDGFRA, PDGFRB
LY2835219	No	473 nM	6.4	16.84	21.95	CDK4, CDK6
SNX-2112	No	287 nM	9.51	16.84	9.58	HSP90AA1, HSP90AB1
ENMD-2076	No	1.5 uM	5.64	16.76	23.45	AURKC
Luminespib	No	1.1 uM	5.95	15.45	8.74	HSP90AA1, HSP90AB1
Osimertinib	Yes	1.7 uM	2.63	12.32	23.74	EGFR
OTX015	No	3.9 uM	1.81	11.75	18.19	BRD2, BRD3, BRD4
Cyclosporine	Yes	1.9 uM	5.34	10.36	0	PPP3R2
Ixabepilone	Yes	153 pM	0	0	24.11	Tubulin
Valinomycin	No	200 pM	0	0	22.84	
Leelamine	No	2 uM	0	0	21.84	
Cladribine	Yes	718 nM	0	0	21.13	POLA1, POLE, POLE2, POLE3, POLE4, RRM1, RRM2, RRM2B
MGCD-265	No	1.1 uM	0	1.76	21.12	FLT1, FLT4, KDR, MET, MST1R, TEK
Vemurafenib	Yes	1 nM	0	0.09	20.66	BRAF, RAF1
Midostaurin	Yes	700 nM	0	4.79	20.62	FLT3, PRKCA
PP-121	No	350 nM	0	0	19.52	PDGFR, HCK, MTOR, VEGFR2, SRC, ABL
Gitoxigenin diacetate	No	70 nM	0	0	19.33	
Octreotide	Yes	5 nM	0	0	19.08	SSTR2, SSTR3, SSTR5
Gambogic acid	No	425 nM	0	0	18.78	
Dactinomycin	Yes	3 nM	0	0	18.52	
Camptothecin	No	4 nM	0	0	18.24	TOP1
Apremilast	Yes	450 nM	0	0	17.61	PDE4, TNF
2,3-DCPE	No	3.5 uM	0	0	17.06	
GSK-3 inhibitor IX	No	3.5 uM	0	0	16.66	GSK3A, GSK3B
Halofuginone	No	1 nM	0	0	16.47	
Cediranib	No	222 nM	0	0	16.41	FLT4, KDR, FLT1, KIT, PDGFRA, CSF1R, FLT3, PDGFRB
Alpelisib	Yes	370 nM	0	0	16.32	PIK3CA, PIK3CB, PIK3CD, PIK3CG
Cabozantinib	Yes	1.1 uM	0	0	16.26	KDR, RET, MET
Axitinib	Yes	144 nM	0	0	15.65	FLT1, FLT4, KDR
Valproic Acid	Yes	2.4 uM	0	0	15.33	HDAC9

Compound	FDA-approved	Concentration	12	24	48	Known targets
Melphalan	Yes	819 nM	0	0	15.15	
Pacritinib	No	573 nM	0	0	14.96	JAK2
Leucovorin	Yes	2.1 uM	0	0	14.53	TYMS
Gentian Violet	Yes	45 nM	0	0	14.45	
Lenvatinib	Yes	647 nM	0	0	14.35	FLT4, KDR, FLT1
Vinorelbine	Yes	2 nM	0	0	14.28	Tubulin
Plumbagin	No	2 uM	0	0	14.12	
Tamoxifen	Yes	1.1 uM	0	0	13.88	ESR1
Azacitidine	Yes	4.1 uM	0	0	13.86	DNMT1, DNMT3A
Alectinib	Yes	1 uM	0	0.25	13.64	ALK
Oxaliplatin	Yes	2.7 uM	0	0	13.4	
PD-166285	No	75 nM	0	0	13.11	SRC, FGFR1, PDGFRB
Bosentan	Yes	833 nM	0	0	12.93	EDNRA, EDNRB
Fulvestrant	Yes	32 nM	0	2.58	12.56	ESR1, ESR2
Raloxifene	Yes	9 nM	0	0	12.55	ESR1
AEE788	No	175 nM	0	0	12.4	ERBB2, KDR, EGFR
Terfenadine	No	2.5 uM	0	0	12.39	HRH1
LY-2183240	No	900 nM	0	0	12.3	FAAH
NSC-95397	No	2.5 uM	0	0	11.97	CDC25A, CDC25C, CDC25B
Toremifene	Yes	1.6 uM	0	0	11.86	ESR1
Zibotentan	No	1.7 uM	0	0	11.73	EDN1
P276-00	No	444 nM	0	1.13	11.53	CDK1, CDK4, CDK9
Gilteritinib	No	2.3 uM	3.26	8.61	11.17	FLT3
Mercaptopurine	Yes	867 nM	0	0	10.96	HPRT1
Momelotinib	No	1.6 uM	5.21	8.45	10.83	JAK1, JAK2
Benzethonium chloride	Yes	5 uM	0	0	10.8	CHRNA4, CHRN2
Lenalidomide	Yes	1.7 uM	0	0.03	10.62	TNF, TNFSF11
Ponatinib	Yes	80 nM	0	0	10.46	ABL1, BCR, FGFR1, KDR, FLT1, TEK, FLT3, FGFR2, FGFR3, FGFR4